



Validation of extreme snow avalanches and related return periods derived from a statistical-dynamical model using tree-ring techniques



Romain Schläppy^{a,*}, Nicolas Eckert^b, Vincent Jomelli^a, Markus Stoffel^{c,d}, Delphine Grancher^a, Daniel Brunstein^a, Mohamed Naaim^b, Michaël Deschatres^b

^a Laboratoire de Géographie Physique, Université Paris 1 Panthéon-Sorbonne, UMR 8591 CNRS, 1 place Aristide Briand, F-92195 Meudon cedex, France

^b IRSTEA, UR ETGR, 2 rue de la Papeterie, BP 76, F-38402 St-Martin-d'Hères cedex, France

^c Dendrolab.ch, Institute of Geological Sciences, University of Berne, Baltzerstrasse 1 + 3, CH-3012 Berne, Switzerland

^d Climatic Change and Climate Impacts, Institute for Environmental Sciences, University of Geneva, 7 Route de Drize, CH-1227 Carouge, Switzerland

ARTICLE INFO

Article history:

Received 17 July 2013

Accepted 1 December 2013

Keywords:

Dendrogeomorphology

Snow avalanche

Runout distance

Return period

Statistical-dynamical model

Hazard zoning

ABSTRACT

Specification of expected runout distances and related return periods are the first and most important steps for zoning in snow avalanche prone terrain. In the past, runout distances of extreme events have often been evaluated with physically- or statistical-based numerical models. More recently, the statistical-dynamical modeling approach has been put forward, as it has the advantage of providing information on avalanche velocity, pressure, and flow depth at each point along a path quantified in terms of probabilities. Most often, calibration of statistical-dynamical modeling is based on existing data from historical archives so that current events with return periods ≤ 30 yr can normally be simulated with high confidence, but uncertainty increases as soon as one wants to deal with longer return periods, thus calling for validation procedures to corroborate model predictions. In this context, we used dendrogeomorphic records of trees impacted by snow avalanches in their runout zone to reconstruct past activity in two avalanche paths of the French Alps. Based on the reconstructed distribution of runout distances of 25 events and mean event frequencies, we successfully derived runout values for events with return periods of ≤ 300 yr. Comparison of relations between runout distance and return periods between dendrogeomorphic data and predictions of a locally calibrated statistical-dynamical model show good agreement. Within the classical intervals used in hazard zoning (i.e. 10–300 yr), mean and mean square errors amounted to ~ 20 and 30–45 m, respectively. These results suggest that dendrogeomorphic time series of snow avalanches can yield valuable information to anticipate future extreme events and that the employed statistical-dynamical model can be used with reasonable confidence to predict runout distances of avalanches with high return periods, despite some uncertainty inherent to the limits of both approaches.

© 2013 Elsevier B.V. All rights reserved.

1. Introduction

Snow avalanches are major hazards to human lives in mountain ranges around the world (McClung and Schaerer, 2006). Mitigation against snow avalanches generally includes analysis of runout distances and related return periods (i.e. the average interval of time within which the runout distance is reached or exceeded at a given location) to designate hazard zones and to design defense structures. Runout distances can be identified through a combination of field observations, historical records, meteorological data or the analysis of aerial photos and topographic maps for vegetation and/or geomorphic evidence (Ancey et al., 2004; Mears, 1992; Weir, 2002). As long and continuous historical observations are generally scarce, the extent of avalanches often needs to be estimated using topographic (or statistic) models (Bovis and Mears, 1976; Eckert et al., 2007b; Keylock, 2005; Lied and Bakkehoi, 1980; McClung and Lied, 1987). These models typically

consist of simple statistical regressions which explain observed runout distances with various topographic covariates. While they allow an estimation of maximum runout distances, they do not, however, provide estimates of avalanche size, speed, force or lateral extent (Delparte et al., 2008).

The more physical characteristics of snow avalanches can, in contrast, be gathered from dynamical models (Voellmy, 1955). Dynamical models require a careful representation of avalanche terrain and internal material properties and can consider interaction between different factors (Mears, 1989). Up-to-date models use the formal framework of continuum mechanics (Savage and Hutter, 1989) to reproduce different types of flows with remarkable accuracy (Bartelt et al., 2012). However, if they are used to simulate single events/scenarios — as generally suggested in the avalanche literature (Salm et al., 1990), they do not allow assessment of uncertainties in runout distance predictions in standard statistical terms (McClung, 1990).

More recently, propagation models and statistical analyses have been coupled explicitly using Monte Carlo simulations and are commonly summarized as statistical-dynamical modeling approaches (Barbolini

* Corresponding author. Tel.: +33 145075581.

E-mail address: romain.schlappy@cnrs-belleveuve.fr (R. Schläppy).

and Keylock, 2002; Bozhinskiy et al., 2001; Eckert et al., 2008b; Keylock et al., 1999; Meunier and Ancey, 2004). Probability distributions are typically chosen for the input variables (e.g., release area and depth, friction coefficient, flow height) and runout distances and related return periods are derived from a large set of model runs. In addition, data on avalanche velocity, pressure and flow depth can be retrieved at each position along the path and quantified in terms of probabilities.

Calibration of statistical-dynamical models with archival records improves the reliability of the approach considerably (Ancey and Meunier, 2004), but data available for calibration typically remains quite limited (Straub and Grêt-Regamey, 2006), non-explicit in nature, and difficult to be implemented in the friction law (i.e. friction parameters may be too numerous for a single solution of the inversion problem; Ancey et al., 2003). Bayesian methods have been used recently to overcome these difficulties, allowing consistent inference and prediction of high return periods with respect to the available information (Ancey, 2005; Eckert et al., 2009; Gauer et al., 2009; Grêt-Regamey and Straub, 2006).

Nevertheless, all models which are currently available are still hampered considerably by imperfect knowledge of the friction law representing snow in motion (Rognon et al., 2008) and difficulties to properly account for transition between different flow types (Issler, 1998). Furthermore, statistical-dynamical models are well capable to simulate contemporary events, corresponding to return period ≤ 30 yr on which they could be calibrated, but uncertainties increase as soon as longer return periods are investigated. A clear need thus exists to validate modeling procedures in order to corroborate model predictions. Recent work has used radar measurements on avalanche test sites (Vriend et al., 2013) to evaluate simulated velocity profiles (Fischer et al., 2013). However, such data from experimental sites will likely yield data on frequent events, but not on extreme runouts corresponding to large/rare events.

On forested paths, dendrogeomorphology (Alestalo, 1971; Stoffel et al., 2010) has been demonstrated to represent a powerful tool to reconstruct past activity of avalanches with annual resolution and for periods covering past decades to centuries (Butler and Sawyer, 2008). The approach is based on the fact that trees form one increment ring per year in temperate climates and that trees affected by mass movements record the evidence of geomorphic disturbance in their growth-ring series (Stoffel and Bollschweiler, 2008; Stoffel et al., 2013). Reactions of trees to snow avalanches are driven by the forces of the avalanche and the mechanical impact of debris (i.e. rocks and boulder or broken trees) transported by the snow as well as by the size and flexibility of the tree itself (Bebi et al., 2009).

Typical reactions of trees to avalanche include tilting, wounding as a consequence of trunk, apex and branch breakage (Bartelt and Stöckli, 2001; Luckman, 2010). These external disturbances are reflected in the wood with anomalous anatomical features, which can be detected and accurately dated in tree-ring series using dendrogeomorphic techniques (Butler and Sawyer, 2008; Stoffel and Bollschweiler, 2008; Stoffel et al., 2013). Assessment of yearly patterns of growth anomalies enables identification of avalanche events based on either quantitative (Butler and Sawyer, 2008; Corona et al., 2012a; Germain et al., 2005; Pederson et al., 2006), qualitative (Stoffel et al., 2006), or semi-quantitative (Schläppy et al., 2013) approaches. Dendrogeomorphic data has been used repeatedly in the past to derive minimum avalanche frequency and magnitude within the path or to estimate avalanche return periods based on disturbance frequency of individual trees (Corona et al., 2010; Reardon et al., 2008).

Even if statistical properties of avalanches in forests (McClung, 2003; Teich et al., 2012) and, for instance, relations between forest terrain and avalanche dynamics (Bartelt and Stöckli, 2001; Feistl et al., 2012; Takeuchi et al., 2011) are now more and more investigated, little attention has been paid to the potential of dendrogeomorphic avalanche records for the calibration or validation of avalanche models so far (Germain et al., 2010). Casteller et al. (2008), for instance, used tree-ring records to validate numerical simulations in Argentina, but not

with a focus on runout distance and/or its relation to return periods in a given path.

Hence, this study represents the first cross-validation of high return period avalanche information derived from a statistical-dynamical model and the long-term, higher-return period information gathered from tree-ring records. Using event chronologies from two avalanche paths located in the French Alps, its aim was to (i) reconstruct past avalanche activity using a semi-quantitative approach and (ii) evaluate runout distances, (iii) calculate return periods of specific events using the mean frequency and runout distance distribution of snow avalanches, and to (iv) compare dendrogeomorphic results with the predictions of extreme avalanches as obtained with a locally calibrated statistical-dynamical model (Eckert et al., 2010c).

2. Study sites

This study was conducted at two sites in the Rhône-Alpes and Provence-Alpes-Côte d'Azur regions of the French Alps, namely at the Avalanche des Pylônes path near Chamonix-Mont-Blanc (Haute-Savoie) and the Château Jouan path near Montgenèvre (Hautes-Alpes; Fig. 1). The selection of the sites was driven by the presence of well localized starting zones of snow avalanches, a straight avalanche path as well as by the existence of stopping zones in forests.

2.1. Château Jouan path

The Château Jouan path (44°55' N, 6°42' E) is located on a N-facing slope of the Durance Valley, 2 km SW of Montgenèvre (Fig. 2a). At the study site, geology is composed of Triassic dolomites and limestones. The nearby meteorological station of Briançon (1324 m asl) records mean annual air temperatures (MAAT) of 7.9 °C (1971–2000) with coolest mean values in January (−4.8 °C). Annual precipitation amounts to 770 mm. Between November and March, precipitation falls primarily as snow, and average annual snowfall reached 258 cm for the period 1961–2001.

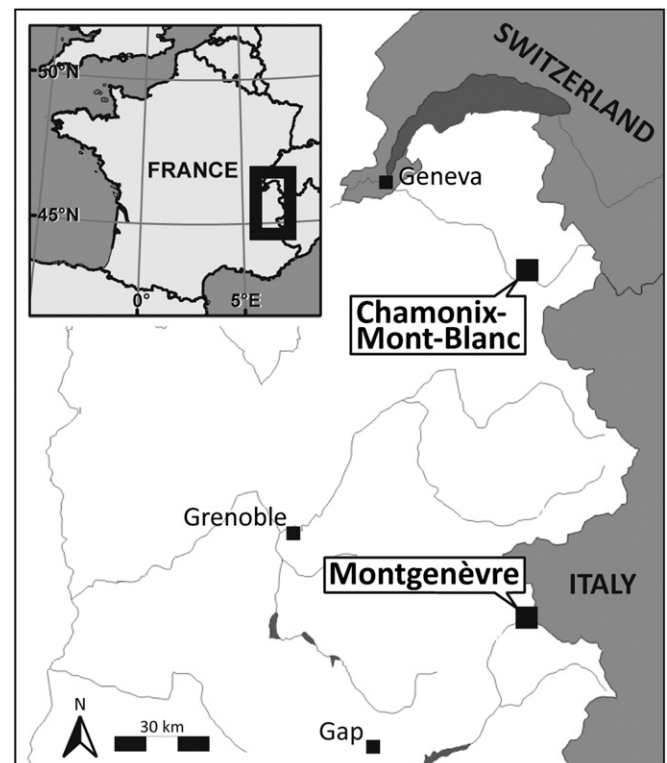


Fig. 1. Location of the Château Jouan (Montgenèvre) and Avalanche des Pylônes (Chamonix-Mont-Blanc) avalanche paths in the French Alps.

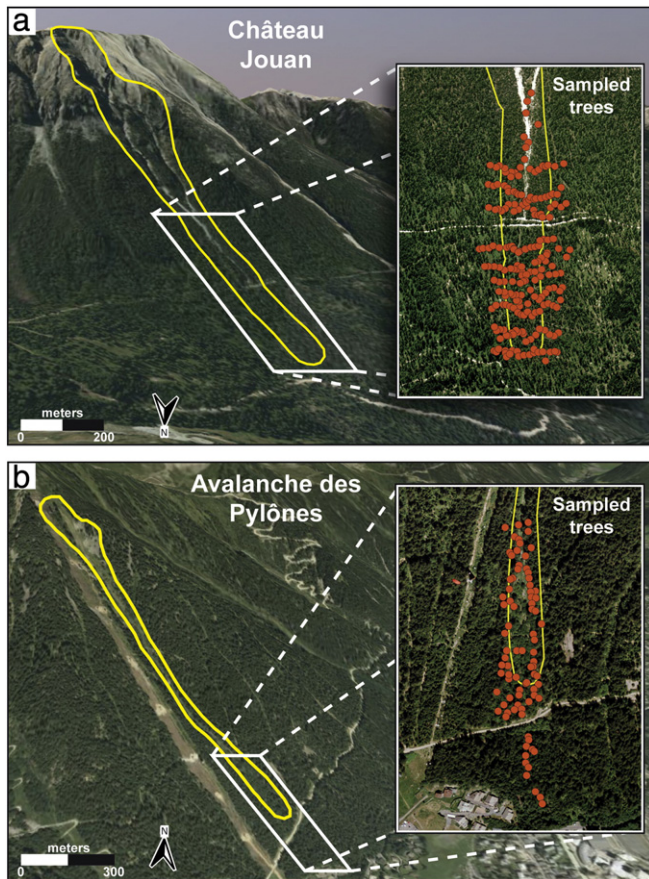


Fig. 2. Localization of sampled trees in the (a) Château Jouan and (b) Avalanche des Pylônes paths.

Snow avalanches are commonly released from a starting zone located at 2500–2100 m asl (mean slope angle: 36°). Avalanches pass a short track before reaching the runout zone at 2000 m asl (mean slope angle: 22°). Vegetation in the upper part of the runout zone is dominated by shrubs and invasive trees species (e.g., *Pinus mugo* subsp. *mugo*), but *Larix decidua* Mill. starts to dominate at 1800–1700 m asl. At 1810 m asl, the path is crossed by a forestry road which is used for cross-country skiing during winter (Fig. 2a).

2.2. Avalanche des Pylônes path

The Avalanche des Pylônes path (45°55' N, 6°51' E) is located on the S-facing slope of the Arve Valley, immediately next to the first section of the Brévent cable car (Chamonix-Planpraz). MAAT at Chamonix-Mont-Blanc (1054 m, asl) was 6.6 °C for the period 1935–1960 and annual precipitation amounts to 1257 mm. Precipitation falls primarily as snow between November and April (average snow cover period: 130 days; Bergue, 2000) and mean annual snowfall was 287 cm (± 121 cm) for the period 1960–2007.

Snow avalanches at the site are generally triggered from a starting zone at 1930–1600 m asl (mean slope angle: 47°). Once released, they pass through an incised path before reaching the runout zone (mean slope: 30°) extending from 1450 m to 1100 m asl. A characteristic transverse vegetation pattern (Malanson and Butler, 1984) can be observed across the starting zone and track. The inner zone is colonized exclusively by shrubs, except for a small scree slope located in the eastern part of the starting zone. In the outer zone, forest vegetation is mainly comprised of *Picea abies* (L.) Karst. with exceptional *L. decidua* and *Alnus viridis*. The runout zone is relatively narrow and trees are very sparse in the central track above 1200 m asl. However, the outer part is covered by a relatively dense forest dominated by *P. abies* with

sparse *Pinus sylvestris* L., *Betula pendula*, *Abies alba* Mill. and some *A. alnobetula* (Bergue, 2000). The path is crossed by a forestry road at 1170 m asl which is used as a skiing track during the winter season. The runout zone ends immediately above the uppermost houses of downtown Chamonix-Mont-Blanc (Fig. 2b).

3. Data and methods

3.1. Avalanche historical data

In France, survey of avalanches was initiated by foresters in the 1900s (Mougin, 1922). Most avalanche events have been recorded in the “Enquête Permanente sur les Avalanches” (hereafter referred to as EPA), containing ~80,000 avalanche events in approximately 3900 recognized paths in the French Alps and the Pyrenees. Data on avalanches are gathered by forest rangers, who also record various quantitative (e.g., runout altitudes, deposit volumes) and qualitative (e.g., flow regime, snow quality) data (Jamard et al., 2002). For safety reasons, rangers do not actually measure runout altitudes, but estimate them from a distant observation point. As a consequence, recorded altitudes are more uncertain than avalanche counts, and have been missed repeatedly because of bad visibility.

All observations are stored in a database and complemented with data on meteorological conditions during the days preceding avalanche occurrence. For each surveyed path, EPA data is usually complemented with a map (Carte de Localisation des Phénomènes Avalancheux or CLPA) localizing the occurrence of avalanches, but these maps usually cover only a limited time span with frequent omissions of past events.

Locally, the quality of EPA records depends to a large extent on the rangers' careful data recording making certain series poor, at least during years corresponding to a ranger's career. In addition, Teich et al. (2012) state that in forested terrain, avalanches are sometimes badly documented as they are not of key importance compared to large destructive avalanches threatening settlements, infrastructure, and human lives in open terrain. More generally, the quality of observations in the different paths is strongly influenced by the potential threat to existing or projected infrastructure and ease of observation (Jamard et al., 2002). Nevertheless, EPA has repeatedly been found a valuable source of information for local scale risk evaluation (Eckert et al., 2008a), the design of defense structures (Naaim et al., 2010), and for larger-scale investigations of avalanche activity and related snow and weather drivers (Eckert et al., 2010a,b; Jomelli et al., 2007).

In this study, we assume that historical records in the Château Jouan and Avalanche des Pylônes paths are sufficient for (i) the calibration of the statistical-dynamical model and for (ii) a comparison of predictions with dendrogeomorphic records. In the Château Jouan path, the first documented event dates back to winter 1926–7. Due to lacking data on type of avalanche, date of occurrence, or runout elevations, we only consider the period 1950–2011 here. In the Avalanche des Pylônes path, the avalanche survey dates back to winter 1985–6. Due to the presence of several critical infrastructures (i.e. cable car, road, houses) in the runout zone of the path, the quality of the avalanche survey is assumed to be satisfying for the period 1986–2012 for which historical archives exist. Note that for both paths, avalanches recorded in the EPA were dense flow avalanches.

3.2. A locally calibrated Bayesian statistical-dynamical model

The Bayesian statistical-dynamical model used in this study has been presented extensively in Eckert et al. (2010c). The main characteristics of the model are summarized in Appendix A. It is based on Saint Venant equations solved numerically along a curvilinear profile $z = f_1(x)$, where z is the altitude and x the horizontal distance starting at the top of the path. The classical Voellmy (1955) friction law is used with its well-known friction coefficients pair, μ and ξ (see Appendix A for more details).

Avalanche frequency a and avalanche magnitude y are modeled as two independent random processes. Avalanche frequency is a scalar discrete random variable corresponding to the number of avalanches recorded each winter and whose long-range mean is necessary for computing return periods (see Section 3.5). Avalanche magnitude is a random vector including all the correlated multivariate quantitative characteristics that vary from one event to another, namely runout distance, velocity and pressure profiles, or snow volume. The probabilistic model is noted $p(y, a | \theta_M, \theta_F)$, indicating that the joint distribution p of the random variables y and a is indexed by parameters (θ_M, θ_F) .

Our data sets $y_i, i \in [1, n]$ and $a_t, t \in [1, T_{obs}]$ corresponding to the n avalanches registered at the study site during T_{obs} years of observation are assumed to be mutually independent. Bayesian inference (Bayes and Price, 1763) combines observations and a prior distribution $\pi(\theta_M, \theta_F)$ which encodes prior knowledge about the unknowns, leading the joint posterior distribution of all parameters and latent variables, as detailed in Appendix B. For each unknown, a point estimate could be derived as well as the related uncertainty quantified by the posterior standard deviation and credibility interval (Table 1, see Appendix A for details of the meaning of each parameter). From the posterior estimates, the posterior distribution of model variables $p(y | \hat{\theta}_M)$ and $p(a | \hat{\theta}_F)$ could easily be obtained (Appendix B).

As discussed in Eckert et al. (2010c), an important point is the need of an informative prior on friction coefficient distributions to grant model identifiability. It is all the more true for our case studies where data quantity is too low to contain enough information to work with poorly informative priors. Many tries were carried out with different prior assumptions resulting from expert knowledge and/or information transfer from other paths. Finally, “strongly” informative priors were found necessary to fit the data in both studied paths (Table 1). For instance, the sensitivity to the a priori distribution on σ , the standard deviation for μ , is very high. In both studied paths, fitting large runouts by combining data and prior information using Bayes theorem was possible only with an a priori little dispersed distribution for σ leading to realistic posterior probabilities for small μ values. Regarding ξ , prior influence is much lower so that prior choice is less difficult. Obtained posterior estimates are, in both paths, relatively close to the prior mean (900), i.e. higher than values proposed in other avalanche simulation studies performed in forested terrain (Bartelt and Stöckli, 2001; Feistl et al., 2012), but lower than those generally used in open grass terrain, in good agreement with the interpretation of ξ in terms of path roughness (Appendix A).

3.3. Dendrogeomorphic analysis and avalanche event reconstruction

In this study, the area sampled with dendrogeomorphic techniques was restricted to the lower track of the path and its runout zone,

as the main goal was to maximize the likelihood of identifying the maximum reach of avalanche events. Sampling was carried out in 2010 and 2011. A total of 438 samples (375 increment cores and 63 cross-sections) were taken from 210 trees at Château Jouan and 187 samples (161 increment cores and 26 cross-sections) were selected from 87 trees at Avalanche des Pylônes (Fig. 2 and Table 2). Sampling was restricted to *L. decidua* and *P. abies*. Characteristic growth disturbances (GD) used to calendar-date the occurrence of past snow avalanches included impact scars (Corona et al., 2013; Stoffel and Perret, 2006; Trappmann and Stoffel, 2013), callus tissue (Schneuwly et al., 2009a; Stoffel et al., 2010) and tangential rows of traumatic resin ducts (TRD; Bollschweiler et al., 2008; Schneuwly et al., 2009b; Stoffel and Hitz, 2008), the initiation of compression wood (Butler et al., 2010; Timell, 1986) and abrupt growth reductions (Butler and Malanson, 1985; Corona et al., 2012a; Kogelnig-Mayer et al., 2013; Stoffel et al., 2013). Selection of trees, sampling design as well as sample preparation and analysis followed the procedures described in Stoffel and Bollschweiler (2008) and Stoffel et al. (2013).

In a subsequent step, intensities were assigned to GDs in order to emphasize features that are clearly associated with avalanche activity and to discriminate these from disturbances possibly induced by other factors (Corona et al., 2012a; Stoffel et al., 2013). GDs were classified based on the visual quality of the evidence of reactions within each sample according to the intensity scale presented in Table 3. GD data from individual trees were then summarized in a geographic information system with ArcGIS (ESRI, 2013). For each year derived from the tree-ring series, trees that were living (i.e. trees present in a given year considering their age as obtained from sample analysis) were plotted according to their geographic coordinates. The determination of snow avalanche years was based on a visual evaluation of the resulting maps and followed the procedure described by Schläppy et al. (2013). Basically, each map (one per chronology year) was assessed separately by analyzing simultaneously the number of disturbed trees present, the proportion of strong intensity GDs compared to intermediate ones as well as their distribution within the path. Weaker reactions were also considered in the yearly assessment and could be helpful in cases where only few disturbed trees were observed. Note that here an avalanche year is related to a winter, with the year 1999 corresponding, for example, to winter 1998–9.

The age structure of the stand was approximated by counting the number of tree rings in all sampled trees and visualized after interpolation. However, as trees were not sampled at the stem base and as their piths as well as the innermost rings were sometimes rotten, the obtained age structure is biased and does neither reflect inception nor germination dates (Corona et al., 2010; Stoffel et al., 2006). Nevertheless, it may provide valuable data on major disturbance events at the study site with reasonable precision, as *L. decidua* has been shown repeatedly

Table 1

Parameters of the statistical dynamical model in the (a) Château Jouan and (b) Avalanche des Pylônes paths. For each parameter, the marginal prior distribution used for Bayesian inference is provided, as well as the posterior mean, the posterior standard deviation and the lower and upper limits of the 95% credible interval.

	Prior	Posterior							
		Château Jouan				Avalanche des Pylônes			
		mean	SD	2.5%	97.5%	mean	SD	2.5%	97.5%
a_1	$a_1 \sim U(0,10)$	0.69	0.23	0.32	1.19	2.25	0.75	1.02	3.87
a_2	$a_2 \sim U(0,10)$	0.9	0.31	0.4	1.62	11.74	4.23	4.82	21.03
b_1	$b_1 \sim N(3,1)$	1.08	0.13	0.82	1.34	1.07	0.15	0.79	1.36
b_2	$b_2 \sim N(0,1)$	0.15	0.25	-0.36	0.64	1.31	0.76	-0.23	2.81
σ_h	$\sigma_h^2 \sim \text{Gamma}(10,100)$	0.32	0.04	0.25	0.4	0.4	0.04	0.33	0.48
c	$c \sim N(0.5,0.2)$	0.49	0.03	0.43	0.56	0.51	0.02	0.46	0.55
d	$d \sim N(0,0.25)$	-0.02	0.05	-0.11	0.07	-0.01	0.06	-0.12	0.1
e	$e \sim N(0,0.25)$	-0.01	0.03	-0.07	0.05	0.05	0.02	0.02	0.09
σ	$\sigma \sim \text{Gamma}(1,0.01)$	0.09	0.01	0.07	0.12	0.05	0.01	0.04	0.07
ξ	$\xi \sim N(900,100)$	873	91	697	1053	1023	67	898	1144
λ	$\lambda \sim \text{Gamma}(0.01,0.001)$	0.31	0.08	0.18	0.48	0.63	0.15	0.36	0.97

Table 2

Sample size, (a) types, and (b) intensity of growth disturbances in the Château Jouan and Avalanche des Pylônes paths.

Sample analysis	Château Jouan		Avalanche des Pylônes	
	Number	Percentage	Number	Percentage
Sampled trees	210	-	87	-
Sample type	438	100%	187	100%
Cross section	63	14%	26	14%
Increment core	375	86%	161	86%
Growth disturbances	491	100%	222	100%
a Impact scars	35	7%	29	13%
TRD [*]	229	46.5%	106	48%
Compression wood	156	32%	36	16%
Growth reduction	63	13%	51	23%
Callus tissue	8	1.5%	0	0%
b Intensity class 5	49	10%	40	18%
Intensity class 4	183	36.5%	138	62%
Intensity class 3	66	13%	5	2%
Intensity class 2	110	22%	19	9%
Intensity class 1	83	18.5%	20	9%

* Tangential rows of traumatic resin ducts.

to recolonize surfaces cleared by snow avalanches and other mass-movement processes in the years following an event (Stoffel et al., 2006; Van der Burght et al., 2012).

3.4. Evaluation of avalanche runout distances from field data

In a first step, we determined runout distances for all historical events based on information contained in the EPA database. We used the minimum runout elevation reported in the EPA to obtain a first idea of the reach of individual avalanches. In a second step, runout distances were estimated for all avalanches identified with dendrogeomorphic techniques, and based on the position of impacted trees within the path. The reach of avalanches in a given year was defined by the location of the lowermost cluster (≥ 2) of trees showing strong or moderate reactions as a result of avalanche disturbance. Reactions in trees scattered below the lowest tree cluster were disregarded to avoid overestimation of runout distances. Noteworthy, trees may record several impacts during the same winter, so the maximum reach obtained with tree-ring records will therefore represent the largest reach and/or extent of all potential events in a given winter.

3.5. Evaluation of return periods

A return period $T_{x_{stop}}$ corresponding to the runout distance x_{stop} (i.e. the T year return level) can be evaluated by combining the annual avalanche rate f (the mathematical expectation of the random variable

Table 3

Growth disturbance intensity scale emphasizing features that are clearly associated with avalanche activity.

Intensity	Growth disturbances characterization
Class 5	Impact scars or dense TRD* which can undoubtedly be associated to a scar.
Class 4	Obvious TRD* (with some gaps in the rows), presence of callus tissue, obvious compression wood being formed for more than 3 successive growth years or abrupt growth reduction lasting for at least 5 years (associated with stem breakage).
Class 3	Obvious compression wood being formed for 1–3 successive growth years following disturbance.
Class 2	Compression wood present but not well defined or growth reduction lasting for less than 5 years.
Class 1	Scattered TRD*.

* Tangential rows of traumatic resin ducts.

$a_t t \in [1, T_{obs}]$, and $F(x_{stop}) = P(X_{stop} \leq x_{stop})$, the cumulative distribution function (cdf) of runout distances:

$$T_{x_{stop}} = \frac{1}{f(1 - F(x_{stop}))} \quad (1)$$

Hence, for both model outputs and field data, estimates \hat{f} and $\hat{F}(x_{stop})$ must be derived. In the Poisson frequency model with single parameter $\theta_F = \lambda$ used in this paper (Appendix A), the mean frequency estimate \hat{f} is simply $\hat{\lambda}$. For field data, rather than considering only the ratio between the total number of avalanche events observed and the related number of years considered in the chronology (i.e. mean frequency), we retained the median of all possible values. The possible values were determined considering the time period for which data quality was considered acceptable and data quantity sufficient to obtain robust estimates of avalanche occurrence rates (see Sections 4.2 and 5 for details). This procedure was applied to both the historical and the dendrogeomorphic records.

On the other hand, $\hat{F}(x_{stop})$, the estimated cumulative distribution function (cdf) of runout distances was approximated using a variation of the Hazen formula (Hazen, 1914), common in hydrology:

$$\hat{F}(x_{stop}) = \frac{j(x_{stop}) + 0.5}{n + 1} \quad (2)$$

where $j(x_{stop})$ is the number of events which stopped before the distance x_{stop} , and n the total number of events observed in a path. This was applied to the historical and tree-ring runout distance datasets, but also to a sample of 20,000 simulations of $p(x_{stop}|\theta_M)$, the estimated distribution of runout distances (see Fig. 3c for Château Jouan).

As a result of the limited number of observations, the estimation of return periods was subject to a considerable level of uncertainty affecting both \hat{f} and $\hat{F}(x_{stop})$. To evaluate and take into account these uncertainties, we (i) as said before computed all possible values of \hat{f} and performed a sensitivity study, and (ii) computed asymptotic non-parametric confidence intervals CI_F for $\hat{F}(x_{stop})$ as follows:

$$CI_F = \hat{F}_{x_{stop}} \pm \frac{q_{N\alpha}}{\sqrt{n}} \times \sqrt{\hat{F}_{x_{stop}} \times (1 - \hat{F}_{x_{stop}})} \quad (3)$$

with $q_{N\alpha}$ the quantile of the standard Gaussian distribution related to the confidence level α (classically 95%). This was done for tree-ring and historical records only, as for model simulations, samples large enough to lower the width of this interval to zero were considered.

For hazard zoning purposes, the inverse problem has to be solved, i.e. the annual exceedance probability is known, for example 0.01 for the centennial event, and the associated runout distance has to be found. Inverting Eq. (1) shows that the T year return level x_{stop_T} is provided by:

$$x_{stop_T} = \hat{F}_{x_{stop}}^{-1} \left(\frac{\hat{f}T - 1}{\hat{f}T} \right) \quad (4)$$

where $\hat{F}_{x_{stop}}^{-1}$ is the inverse cumulative distribution function of the considered runout sample. For the different samples, $\hat{F}_{x_{stop}}^{-1}$ was evaluated by kernel smoothing of the empirical inverse step function. This has the advantage to avoid using Hazen (Eq. (2)) or other similar approximations, and provides smoother runout distance–return period relations as compared to the direct use of Eq. (1). Note that Hazen formula was nevertheless used to evaluate the maximum empirical return period for each event of the tree-ring and historical chronicles in the two studied paths, and to obtain bounds for computing the confidence interval around the runout distance–return period relationships.

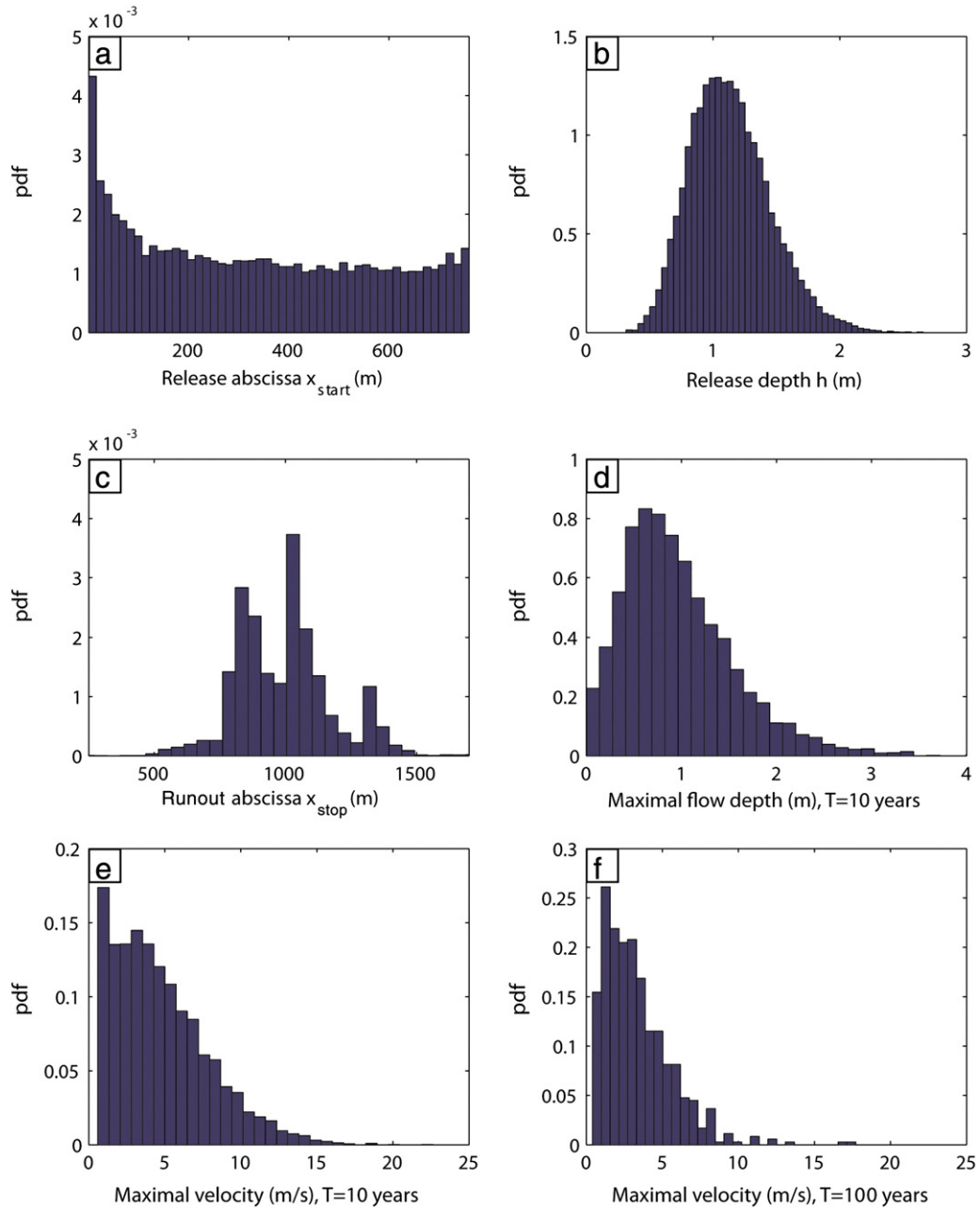


Fig. 3. Multivariate statistical-dynamical avalanche model fitted on the Château Jouan EPA data. (a) release abscissa distribution. (b) release depth distribution. (c) runout distance distribution. (d) maximal flow depth distribution for avalanches whose runout distance exceeds the 10-yr return period abscissa. (e-f) maximal velocity distribution for avalanches whose runout distance exceeded the (e) 10-yr and (f) 100-yr return period abscissas.

Noteworthy, the joint distribution of the exceedance $p(y|\theta_M, x_{stop} > x_{stop_T})$ provided by the statistical-dynamical model, summarizes the characteristics of all avalanche events at the abscissa x_{stop_T} . It can therefore be considered as the joint distribution of all reference scenarios corresponding to the return period T (Fig. 3e-f for maximum flow depths and velocities at the 10-yr return period abscissa and maximum velocities at the 100-yr return period abscissa in the Château Jouan path, respectively).

3.6. Cross validation of model's simulations with independent dendrogeomorphic data

As summarized in Fig. 4, the cross validation of model simulations and dendrogeomorphic chronicles is performed through the calculation

of $\bar{\delta}$, the mean error, and $\bar{\delta}_2$, the (root) mean square error, between return levels derived from both methods:

$$\bar{\delta} = \frac{1}{(T_{\max} - T_{\min} + 1)} \times \sum_{T=T_{\min}}^{T_{\max}} (x_{stop_{model}}(T) - x_{stop_{dendro}}(T)) \quad (5)$$

$$\bar{\delta}_2 = \frac{1}{(T_{\max} - T_{\min} + 1)} \times \left[\sum_{T=T_{\min}}^{T_{\max}} (x_{stop_{model}}(T) - x_{stop_{dendro}}(T))^2 \right]^{1/2} \quad (6)$$

where $x_{stop_{model}}(T)$ and $x_{stop_{dendro}}(T)$ are the runout distances related to return period T derived from the model and tree-ring reconstruction,

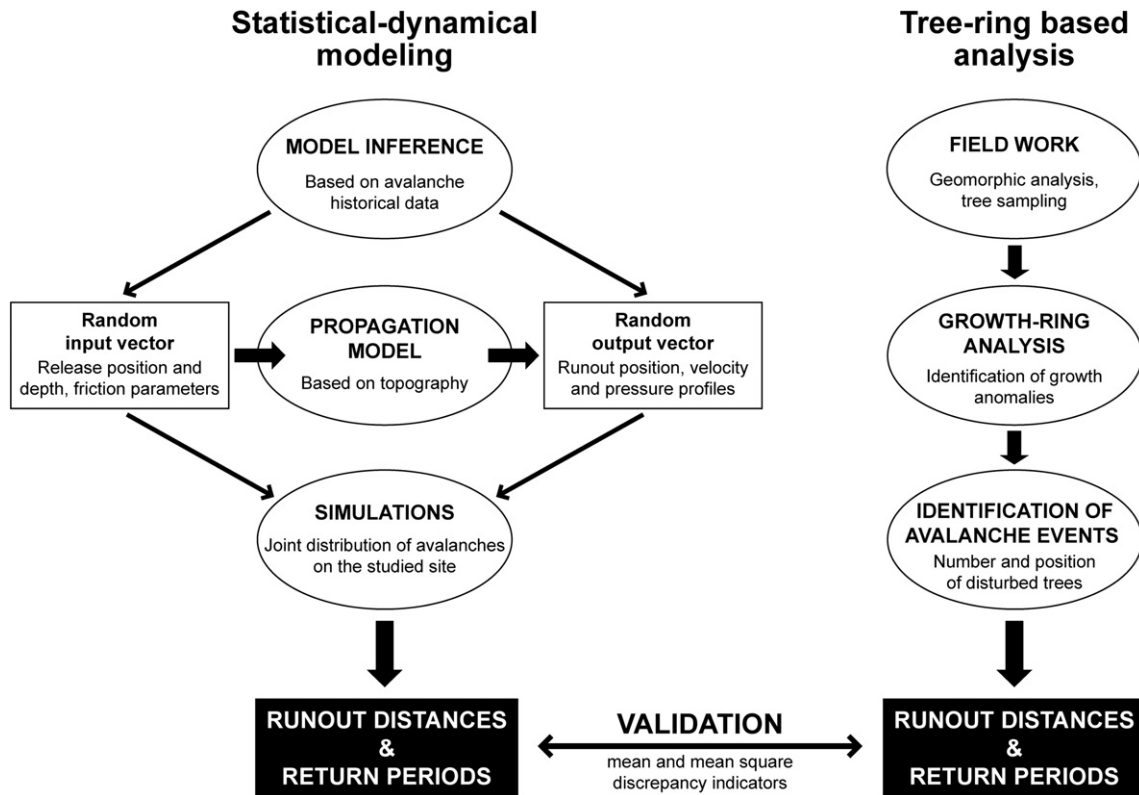


Fig. 4. Flowchart of the principal steps leading to the cross validation of runout distance-return period relationships.

respectively, and $[T_{min}, T_{max}]$ the return period range on which the comparison is made.

The mean error on a given return period range corresponds to the mean value of the positive and negative errors on this range without considering its sign. In our case, a positive mean value implies that

simulated runout distances are larger on average than empirical ones for the $[T_{min}, T_{max}]$ return period interval, and vice versa. However, independently from the sign, a low mean value can result from the compensation between overestimations and underestimations from the model. Consequently, a bias tending to zero provides no information

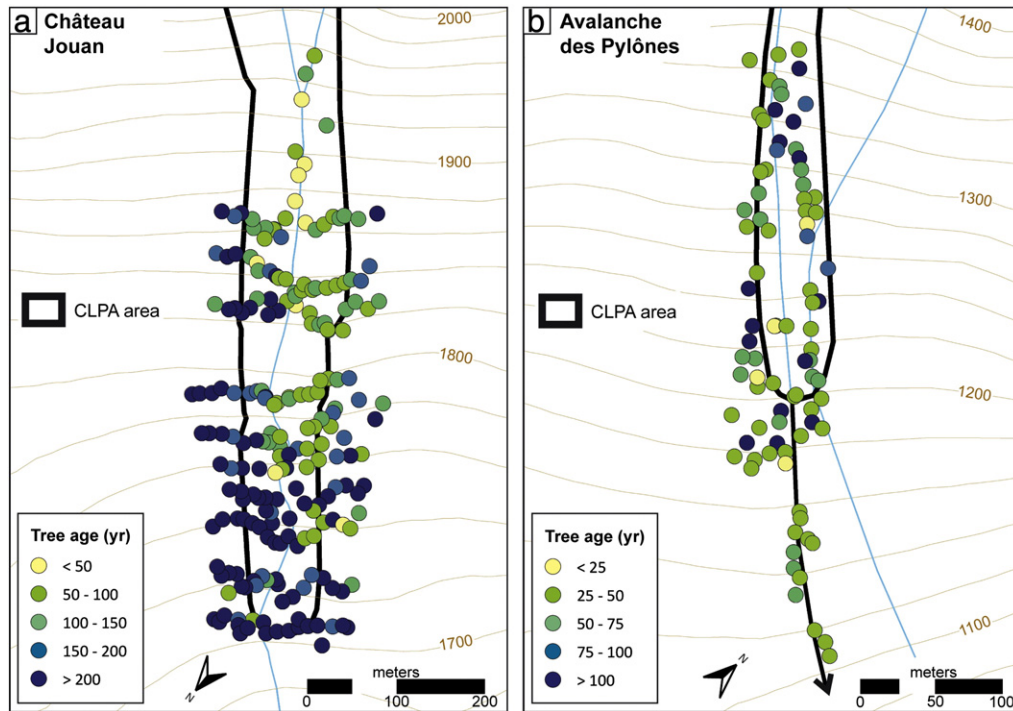


Fig. 5. Age structure of the forest stand growing in the (a) Château Jouan and (b) Avalanche des Pylônes paths as obtained from tree-ring data. Tree ages were approximated by counting the number of tree rings present in the selected trees and at sampling height. The black arrow corresponds to the maximal reach of very shallow avalanche flows that have been recorded in the EPA data.

about the effective dispersion of errors around the mean value. For this reason, we also calculated the mean square error, which takes into account the average of the squares of the errors. In this case, a low value means that all observed bias were relatively low or tend to zero, indicating that simulations and observations are really similar on the $[T_{min} T_{max}]$ range.

4. Results

4.1. Tree-ring analysis and event reconstruction

4.1.1. Age structure of the forest stand

At Château Jouan, sampled trees have an average age of 160 ± 70 yr at sampling height. The oldest tree reached sampling height in AD 1712 and the youngest one in 1992. A total of 92 trees were at least 200 yr old. Ages of trees tend to increase from the lower portions of the avalanche track to the lower segments of the runout zone (Fig. 5a). In a similar way, tree ages gradually increase from the inner to the outer zones of the path. This spatially heterogeneous tree age distribution indicates that major parts of the stand might have been eliminated by large snow avalanches in the past.

In the Avalanche des Pylônes path, data on the pith age at sampling height indicates a mean age of trees of 65 ± 52 yr. The oldest tree reached sampling height in AD 1770 and the youngest one in 1994. Fig. 5b nicely illustrates that tree age distribution within the path is relatively homogeneous. As a consequence, we may assume that most avalanches remained confined to the inner part of the path and were not of sufficient magnitude to destroy major portions of the forest stand.

4.1.2. Growth disturbances and identification of avalanche events

Sample analysis permitted identification of 491 and 222 GD, respectively, in the Château Jouan and Avalanche des Pylônes paths (Table 2). The formation of TRD following cambium wounding and the onset of compression wood after tilting were commonly found in the samples, but abrupt growth reductions, impact scars as well as callus tissue were also present. Most of the GD are of moderate and strong intensities, but slightly less intense at Château Jouan (59.5%) than at Avalanche des Pylônes (82%; Table 2).

Based on the yearly distribution of reacting trees within the path, 13 avalanche events were identified in the Château Jouan path for the period 1799–2010 (Table 4). The temporal distribution of avalanche events was relatively homogeneous since 1910 with 1–3 avalanche winters per decade. Somewhat less activity is observed in the 1940s and 1990s. Only two avalanche winters can be dated prior to the 20th century, namely in 1873 and 1799. In the Avalanche des Pylônes path, 12 avalanche winters were identified for the period 1963–2011

(Table 4). The temporal distribution of avalanche winters is quite homogeneous on this period, but small gaps exist for most of the 1970s and between 1999 and 2006.

4.2. Determination of event frequencies

Mean event frequencies in both paths are relatively constant over long time periods (Fig. 6). In the Château Jouan (Avalanche des Pylônes) path, the median of all possible values amounted to 0.09 (0.22) for the tree-ring based event chronology and to 0.32 (0.59) for the historical archives (Fig. 6, Table 5). Fig. 6d and h also indicate the upper and lower plausible values (2.5 and 97.5% of the histograms) which will be used later to evaluate the influence of value choices on the comparison between empirical and simulated return periods.

4.3. Runout distance distribution along the path

At Château Jouan, runout altitudes existed for 16 avalanches recorded accurately in the EPA database and ranged from 2100 to 1750 m asl. Runout altitudes estimated for the 13 avalanches reconstructed with tree-ring records ranged from 1840 to 1710 m asl (Table 4). At Avalanche des Pylônes, runout altitudes from 15 EPA events varied between 1450 and 1100 m asl, whereas the values derived from dendrogeomorphic data ranged from 1340 to 1120 m asl (Table 4). Based on the runout altitude data, we estimated runout distances and represented related empirical cumulative distribution functions (cdf) graphically. Fig. 7 illustrates runout distances and indicates that the data obtained from the EPA principally informs about small to medium avalanche events, whereas the information derived from dendrogeomorphic reconstructions rather focuses on avalanches with larger spatial extent. This was particularly well illustrated in the Château Jouan path where 50% of the avalanche events reported in the EPA archives stopped before the first event identified in the tree-ring reconstruction (Fig. 7a).

Due to the fact that model calibration was based on avalanche data as reported in the EPA, cdfs derived from the simulations are quite similar to those derived from the database of historical events for small and intermediate runout distances (Fig. 7). Conversely, for larger events, model output tends to look more like runout distances derived from dendrogeomorphic records, and thus confirms the appropriateness of tree-ring records to test extreme predictions.

4.4. Cross validation between simulated and empirical high return periods

Based on mean event frequencies \hat{f} and estimated cumulative distribution functions $\hat{F}(x_{stop})$, return periods corresponding to all historical and tree-ring based events were then evaluated using Eqs. (1–2). At Château Jouan, return periods related to historical events ranged from 3 to 100 yr (Fig. 8a). By contrast, runout distances derived from dendrogeomorphic data corresponded rather to large extent events with return periods >300 yr ($T_{max} = 311$ yr). Conversely, less information was obtained for small events, since the minimum return period that could be derived from the tree-ring record was >10 yr ($T_{min} = 12$ yr). At Avalanche des Pylônes, return periods obtained from the EPA database varied between 2 and 54 yr (Fig. 8b), whereas dendrogeomorphic records informed about return periods trespassing 100 yr ($T_{max} = 118$ yr).

However, although these discrete values may give an approximate idea of empirical return period distributions along the paths under investigation, it must be stressed that the related uncertainty level remains high due to the limited number of available data, as is illustrated by the 95% confidence intervals represented in Fig. 9. This explains why, even if the true runout distance–return period relationship in one given path is unique, at a given position along the path, corresponding return period from historical EPA archives may differ slightly from the one derived from tree-ring data. In that sense, uncertainty increases rapidly

Table 4

Tree-ring based snow avalanche events, minimum runout altitudes and related horizontal runout distances in the Château Jouan and Avalanche des Pylônes paths.

Snow avalanche events					
Château Jouan			Avalanche des Pylônes		
Event year	Runout altitude (m)	Horizontal runout distance (m)	Event year	Runout altitude (m)	Horizontal runout distance (m)
2009	1840	1058	2006	1120	1136
2007	1790	1192	1999	1230	914
2004	1760	1271	1997	1200	968
1986	1740	1339	1992	1200	968
1977	1760	1271	1990	1270	830
1963	1830	1085	1986	1270	830
1960	1780	1218	1982	1180	1005
1951	1770	1243	1980	1200	968
1934	1790	1192	1979	1340	719
1930	1820	1111	1970	1270	830
1919	1750	1302	1966	1190	986
1873	1780	1218	1963	1190	986
1799	1710	1444			

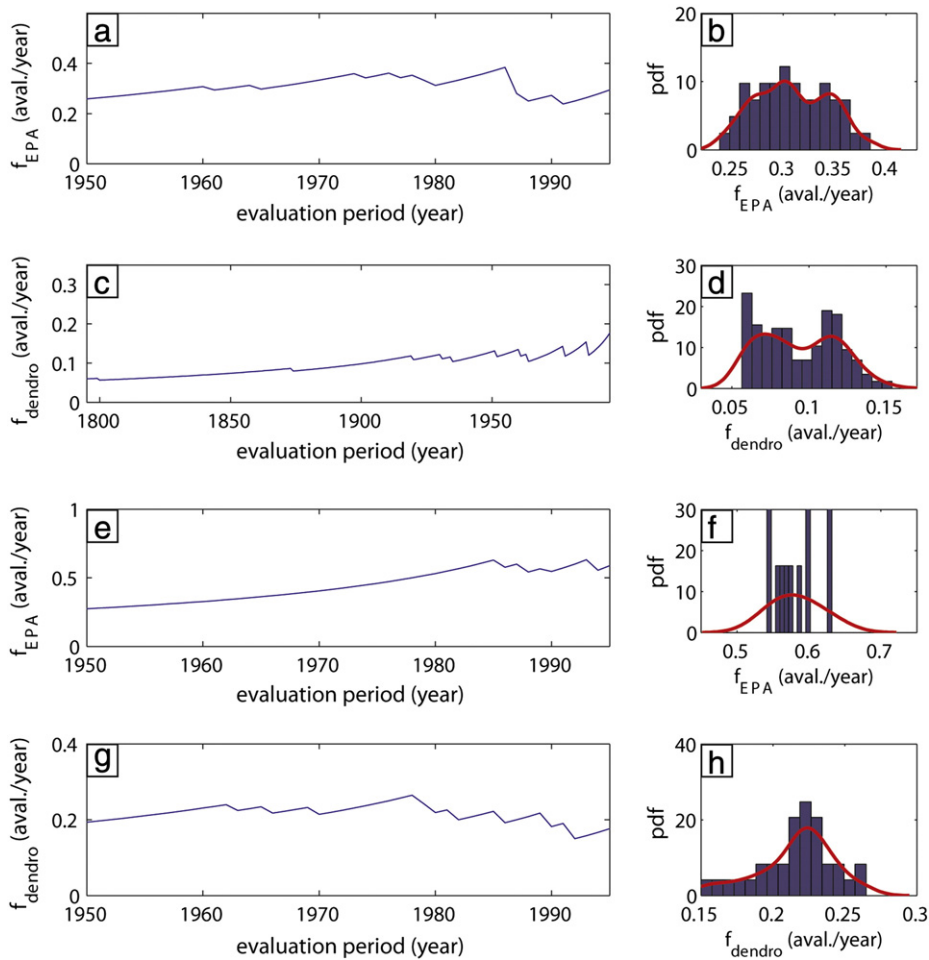


Fig. 6. Evaluation of annual mean frequency in the (a-d) Château Jouan and (e-h) Avalanche des Pylônes paths: (a, e) annual frequency for historical events as a function of the considered time window. (b, f) related probability distribution. c, g) annual frequency for dendrogeomorphic events as a function of the considered time window. (d, h) related probability distribution. In this work, for the historical and tree-ring based chronicles, the median of histograms 6b, 6f, 6d, and 6h were primarily considered (Table 5).

with runout distance for both the historical (EPA) and dendrogeomorphic records in both paths. At Château Jouan, for example, runout distances related to 30-yr and 100-yr return periods derived from tree-ring data are between 1200–1352 m and 1271 m and $+\infty$ m, respectively.

Noteworthy also, the maximum runout distance related to EPA events was reached twice during the period of observation in both studied paths. Consequently, the corresponding return period is somewhat undetermined, leading to a vertical ending of the corresponding runout distance–return period relationships and to even higher uncertainty levels for high return periods evaluated with historical archives.

Because the return periods reported above were evaluated with the Hazen approximation, introducing an additional source of uncertainty for very high return periods, we rather compared runout distance–return period relations as derived with the model simulations and dendrogeomorphic data using the inverse cumulative distribution function (cdf) of the considered runout sample (Eq. (4)). Analysis

Table 5

Historical and tree-ring based annual event frequencies. Considered median annual frequency and related 2.5%, and 97.5% were derived from Fig. 6.

Path name	Chronology type	Annual frequency 2.5%	Annual frequency median	Annual frequency 97.5%
Chateau Jouan	Historical archives	0.26	0.32	0.38
	Tree-ring data	0.06	0.09	0.14
Avalanche des Pylônes	Historical archives	0.54	0.59	0.7
	Tree-ring data	0.18	0.22	0.26

included the mean and mean square errors for both paths and different return period ranges, according to data availability.

In the Château Jouan path, such a comparison was possible for return periods ranging roughly from 10 to 300 yr, corresponding to the classical interval used in hazard zoning (Fig. 9, Table 6). Mean and mean square errors amounted to 19.7 and 28.9 m, respectively, which can be considered satisfying considering the different uncertainty sources that exist in this kind of analysis regarding data or model and with respect to the context of avalanche zoning problems. The best fit is observed for the range of 100–300 yr, for which the mean error amounted to only 20.0 m and the mean square error to 23.8 m (Table 6). Larger discrepancies were found for the range of 10–30 yr with a negative value obtained for the mean error (–36.2 m), reflecting the fact that runout distances derived from tree-ring records are larger for this range of return period than the one derived from the model. Results for the 10–1000 yr return period range were similar to the range of 10–300 yr, given that only nine additional return periods were available for the tree-ring based runout distance–return period relationship ($T_{max} = 309$ yr).

In the Avalanche des Pylônes path, comparison was mostly limited to return periods ranging from 10–100 yr, given the empirical $T_{max} = 118$ yr. However, for the purpose of comparison, we also calculated mean and mean square errors over the same intervals as in the Château Jouan path. As a consequence, mean and mean square errors are the same for the 10–300 and 10–1000-yr return period intervals, amounting to 23.5 and 45.8 m, respectively (Table 6). In more detail, for the return period interval 10–30 yr, errors amount to roughly

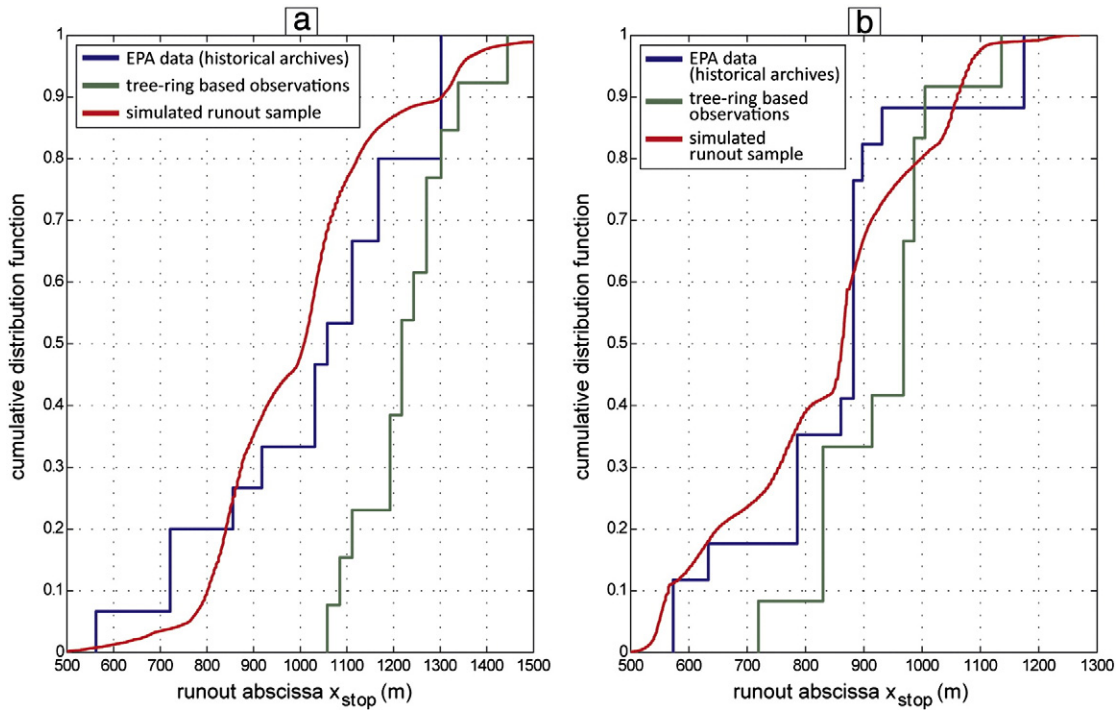


Fig. 7. Empirical and simulated cumulative distribution functions (cdf) of runout distances in the (a) Château Jouan and (b) Avalanche des Pylônes paths.

80 m, indicating that the model and tree-ring data are not in good agreement. Errors start to decrease with increasing ranges of return periods: for the interval 30–100 yr, errors are 17.1 and 36.1 m, respectively. The best fit was found for the interval 100–300 yr, with mean and mean squared errors equal to -18.0 and 18.1 m, respectively. However, these values should be interpreted cautiously as they only reflect discrepancies between simulated and tree-ring data for the interval 100–118 yr, according to T_{max} .

5. Discussion and conclusion

Specification of expected runout distances and related return periods in the runout zone has been defined as the first and most important step for zoning in snow avalanche prone terrain (McClung, 2000). As a consequence, runout distances of extreme events have often been evaluated using physically based numerical models in the past. More precisely, the rationales of Salm et al. (1990) were thereby largely used by practitioners to evaluate “high magnitude” runout distances,

in a rather efficient way but without an explicit statistical framework (Ancy et al., 2004). More recently, statistical-dynamical modeling approaches have been put forward as an alternative approach, where calibration is based on local data reported in historical archives – EPA in the present case – and where probabilistic simulations enable local evaluation of return period at any point along a given path (Eckert et al., 2008b, 2010c).

In this study, a statistical-dynamical approach has been used to analyze runout distances at two avalanche sites in the French Alps, Château Jouan and Avalanche des Pylônes. According to historical data available in the EPA, the model was capable to simulate current events with relatively small return periods (i.e. ≤ 30 -yr return interval). As validation of simulated data could not be realized for higher return periods with EPA data, we reconstructed runout distances of larger, and less frequent, avalanches in both paths with dendrogeomorphic techniques (e.g., Corona et al., 2012a; Schläppy et al., 2013; Stoffel and Bollschweiler, 2008). The dendrogeomorphic record of snow avalanches yielded runout information for 25 avalanche winters in the paths (Table 4), and thus allowed

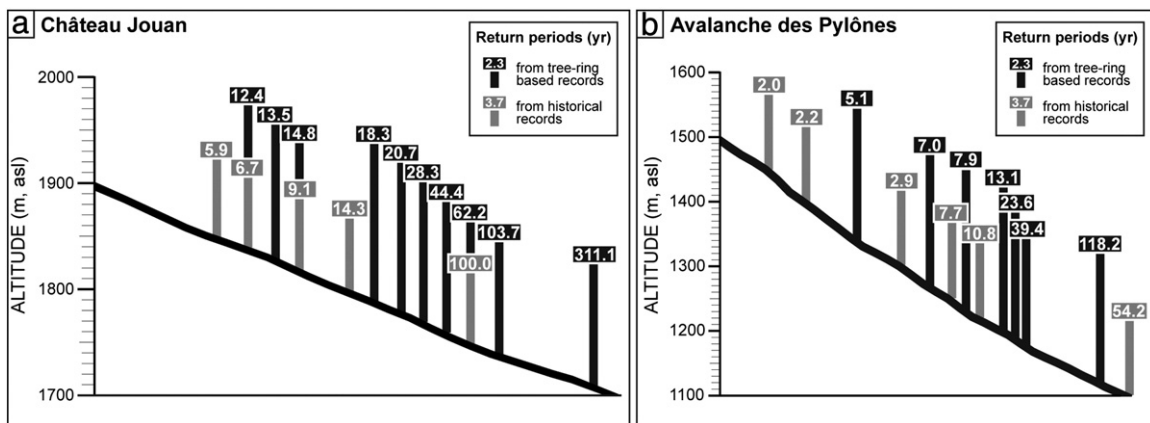


Fig. 8. Return periods (in yr) for each of the historical (grey) and tree-ring based (black) events in the (a) Château Jouan and (b) Avalanche des Pylônes runout zones. Return periods were evaluated based on mean event frequencies (Table 5) and the estimated cumulative distribution function (cdf) of runout distances (Eq. (2)). Note that very small return periods (<5.9 yr) are not represented to simplify display.

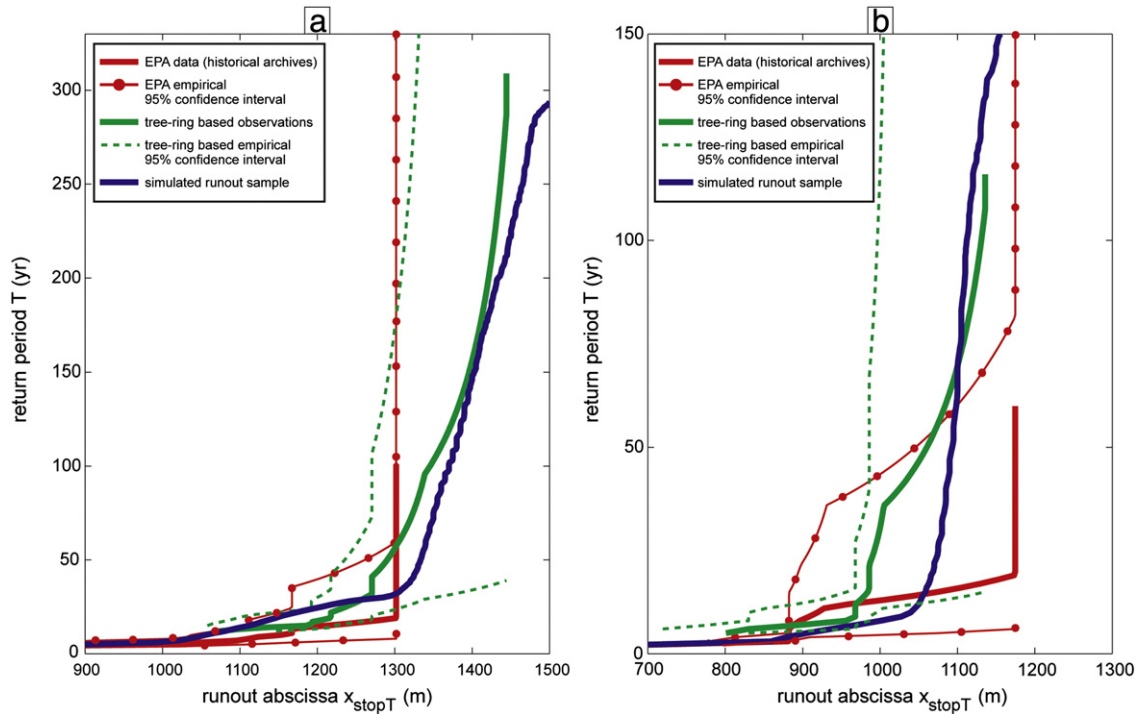


Fig. 9. One-to-one relation between runout distance and return period. Empirical relations and associated 95% confidence intervals derived from historical archives and tree-ring reconstructions are compared to the ones derived from the statistical-dynamical simulations. (a) At Château Jouan, return periods derived from dendrogeomorphic analysis tend to approximate very well modeled data, especially for return periods ranging from 30 to 300 yr. (b) At Avalanche des Pylônes, tree-ring based return periods ranging from 50 to 110 yr correspond roughly to those simulated by the model.

reconstruction of local event chronologies of high-magnitude events as well as estimation of return periods for each of the 25 events using the local runout distance distribution and event frequency as estimated from the tree-ring samples. Comparison of runout distance–return period relations between the simulated data and dendrogeomorphic records showed good agreement on return period ranges for which tree-ring information was available, i.e. for return periods from 10–300 yr and 30–100 yr for the Château Jouan and Avalanche des Pylônes paths, respectively. At both sites, results clearly illustrate the interest and added value of the combined use of statistical-dynamical simulations and tree-ring reconstructions, in particular, for return period ranges which are of interest for avalanche engineering, but not usually covered in historical (EPA) archives. However, we are aware that many sources of uncertainty were involved in the approach used in this paper and should thus be taken into account during the evaluation of the main outcomes. We tried to take them into account as much as possible by using non-parametric confidence intervals and sensitivity analysis to the mean event frequency determination. However, because

of the inherent difficulty of working with extreme events and old (historical chronicles) or indirect (tree-ring reconstruction) data, all sources of uncertainty could not fully be assessed in a quantitative way.

First of all, uncertainties may result from the physical and probabilistic modeling assumptions, as partially discussed in Appendix A (interpretation of the Voellmy' equation), and, in more details, by Eckert et al. (2010c). Among these, subjectivity introduced into analysis by the friction coefficients *prior* choice should be kept in mind while considering the interest of our results for avalanche hazard mapping purposes. For instance, to fit our data to the paths under investigation, imposing an *a priori* low dispersed distribution for σ (the standard deviation of μ) could not be avoided because of the small size of the available historical chronicles, which will obviously reduce the strength of our results in view of a possible application of statistical-dynamical models on poorly documented sites. At the same time, however, the same *prior* choice yielded the best results among numerous trials (not presented in this paper) on both paths. Furthermore, the necessity of its use may reflect nothing more than the so-called Weibull (bounded) attraction domain of extreme avalanches that has been documented for the few datasets where it could be estimated (Ancy, 2012; Keylock, 2005). Hence, the strongly informative *prior* put forward in this study may well be a robust choice for a first approximation in various other paths.

Second, determination of a mean event frequency represents a crucial analytical step as it influences the evaluation of empirical return periods and, consequently, their comparison with model simulations. The sensitivity of the comparison was performed for the Château Jouan path, where the tree-ring chronology is much longer as compared to Avalanche des Pylônes. On the range $f = 0.06$ – 0.14 (Fig. 6c–d), the bias between methods tends to become increasingly negative with increasing values of f (Fig. 10a) which “mechanically” increase tree-ring based runout distance corresponding to given return periods. The tree-ring event frequency value which minimizes the mean square error with model simulations is $f = 0.102$, and thus similar to the value selected for this path ($f = 0.09$, the median over all possible values). Furthermore, fluctuations between the tree-ring based runout

Table 6

Mean and mean square errors between tree-ring based runout distance–return period relations and model simulations as functions of time windows. For each time window, the number of years for which the tree-ring based estimation could be evaluated is provided.

Path name	T_{min}	T_{max}	δ runout distance	δ_2 runout distance	number of years with a tree-ring based estimate on the [T_{min}, T_{max}] interval
Château Jouan	10	300	19.7	28.9	289
	10	30	−36.2	46.2	19
	30	100	34.0	35.1	71
	100	300	20.0	23.8	201
	10	1000	21.7	32.2	298
Avalanche des Pylônes	10	300	23.5	45.8	107
	10	30	79.6	79.7	21
	30	100	17.1	36.1	71
	100	300	−18.0	18.1	17
	10	1000	23.5	45.8	107

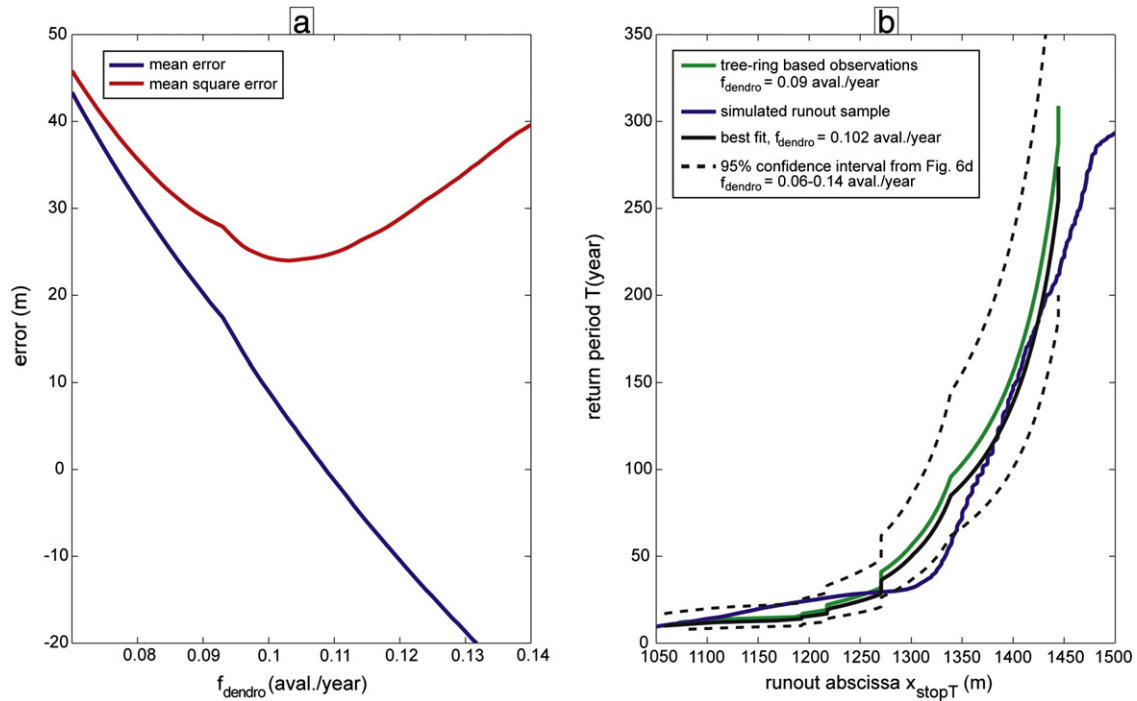


Fig. 10. Influence of the tree-ring based event frequency on the comparison for the Château Jouan path: (a) mean and mean square errors as functions of the tree-ring event frequency. (b) tree-ring based runout distance–return period relations versus model simulations for the range of possible mean event frequencies from Fig. 6c-d.

distance–return period relations, where f varied between 0.09 and 0.102, and modeled data were inferior to 10 m on average (Fig. 10). Consequently, using the median of all possible values as a mean event frequency does not only seem relevant but also yields fairly robust results.

The evaluation of empirical return periods also depends on the cumulative distribution function (cdf) of observed runout distances. Rather than using the classical Hazen formula or other techniques used for the estimation of empirical exceedance probabilities, we calculated $x_{\text{stop}T}$ using the inverse cdf of the considered runout sample (Eq. (4)) so as to minimize the uncertainty level related to the limited number of available data.

This study did not, by contrast, quantify the influence of the quality of the historical and dendrogeomorphic event chronologies. These could have been addressed as well, as recent studies highlighted that tree-ring reconstructions tend to underestimate the number of years with natural avalanche activity by up to 60% (Corona et al., 2010, 2012a; Schläpky et al., 2013), and that avalanche chronicles, such as the EPA, may have observational gaps or records of limited quality. As a matter of fact, both the historical and dendrogeomorphic mean event frequencies might have been underestimated, which, in turn, may affect the evaluation of empirical return periods. At the same time, however, and as high return period events tend to cause significant damage to infrastructure and/or forest, the likelihood that they have been missed in historical archives or not been recorded by the trees is unlikely. As a consequence, and as reported by Corona et al. (2012a), Stoffel and Bollschweiler (2009) and Stoffel et al. (2013), the resulting bias is supposed to influence preferentially small return periods (≤ 30 yr) which typically correspond to current events. Indeed, the agreement between model and tree-ring data has been shown to be somewhat limited for this return period range, but much more conclusive for larger ranges. In consequence, we assume that this source of uncertainty will be rather limited for return periods varying between 30 and 300 yr, i.e. for the interval which is of much more relevance for long-term avalanche forecasting.

Another source of uncertainty results from the estimation of runout distances based on the position of impacted trees within a path, as

dendrogeomorphic reconstructions have been reported to possibly underestimate runout distances in some cases (Corona et al., 2012a). This underestimation is mainly due to changes in path geometry (steepness, curvature) as well as to the presence of a forest stand in the runout zone that can induce rapid avalanche deceleration (McClung, 1990; McClung and Schaerer, 1985). As a consequence, snow pressures may be insufficient in these zones to damage trees and thereby cause reactions in the tree-ring record, particularly at the front of the deposit. In addition, the sampling strategy can also influence the accuracy of runout distance estimation. Given that the sampled trees are generally selected along transects across the slope (Fig. 5a), one might underestimate runout distances of avalanches stopped between two transects and possibly explains the negative bias observed between runout distances for return periods of 30–300 yr (Fig. 9a) derived from tree-ring records and those obtained with simulations in the Château Jouan path.

We also assumed in this study that an underlying stationary process would generate high-magnitude snow avalanche events, as, despite of a clear climate control of avalanche occurrences (Castebrunet et al., 2012), long-term changes in avalanche activity could not have been found in most observational records (Laternser and Schneebeli, 2002). We did not, therefore, include the findings of Eckert et al. (2013) who observed, based on EPA data, a recent and accelerated reduction of high return period avalanches in the French Alps which could possibly be linked with a decrease of snow cover and changes in preferred avalanche types under climate warming (Martin et al., 2001). In addition, climate change since the end of the Little Ice Age as well as changes in land use are likely to have had considerable impacts on both forest cover and avalanche activity on the longer term as well (Jomelli and Pech, 2004), but have not been considered in the context of this study either. As a consequence, the frequency and magnitude of destructive forest avalanches may have been larger or smaller in the past, but signs of such changes are not obvious in the investigated paths where the total number of events reconstructed with tree-ring records was only large enough to see that the number of recorded events decreases with time and at a pace similar to the decrease of the sample size of trees available for dendrogeomorphic analyses (Stoffel et al., 2013). We call for future work where non-stationary statistical-dynamical simulations

are implemented and, if possible, confronted with longer and more abundant tree-ring chronicles to take climate and land-use change effects into account as well (Corona et al., 2012b).

All in all, despite the various sources of uncertainty, we are convinced that this contribution is of high value as it provides, for the first time, a rather conclusive cross-validation of runout distance–return period relations derived from a statistical-dynamical model with data derived from independent, natural archives. Hence, dendrogeomorphic data can be seen as an extremely valuable data pool for the assessment of runout distances and return periods of extreme avalanche events, and in particular for the hazard zoning on forested paths with limited or no historical data. At the same time, we illustrate that the statistical-dynamical model presented here can be used with reasonable confidence to predetermine high return period avalanches and associated information on avalanche velocity, snow pressure and snow depth. Furthermore, it is hoped that the information contained in tree-ring records could be used in the future to evaluate the various modeling assumptions related to weight and sensitivity for high return periods as well as velocity and/or pressure distributions within the statistical-dynamical set-up, and to propose subsequent model improvements.

Acknowledgements

The authors gratefully acknowledge Louis Manière and Matthieu Schläpky for their assistance in the field. They also want to thank the Office National des Forêts (ONF) for sampling permissions. This study has been realized within the framework of the MOPERA (MODélisation Probabiliste pour l'Evaluation du Risque d'Avalanche) program funded by the French National Research Agency (ANR-09-RISK-007-01). R.S. acknowledges support from the Swiss National Science Foundation (project P1SKP2_148492). Finally, the authors are grateful to J. Schweizer, P. Gauer and two anonymous referees whose constructive comments helped to improve the paper.

Appendix A. Statistical-dynamical model

Following Naaim et al. (2004), dense avalanche flow propagation is modeled with depth-averaged Saint Venant equations, but, to facilitate the specification of the input conditions corresponding to each simulation and to reduce computation times, snow incorporation and deposition are ignored. Variation in the momentum corresponds to the difference between gravity g and the robust (e.g., able to produce reasonable results in most occasions) Voellmy (1955) friction law. The equations of mass and momentum conservation in which v is the flow velocity, h is the flow depth, ϕ is the local slope, and t is time are then:

$$\left. \begin{aligned} \frac{\partial h}{\partial t} + \frac{\partial(hv)}{\partial x} &= 0 \\ \frac{\partial(hv)}{\partial t} + \frac{\partial}{\partial x} \left(\alpha_{sv} h v^2 + k_{sv} g \frac{h^2}{2} \right) &= h \left(g \sin \phi - \mu g \cos \phi - \frac{g}{\xi h} v^2 \right) \end{aligned} \right\} \quad (7)$$

k_{sv} represents the ratio between the stress normal to the slope and the stress parallel to the slope, and α_{sv} represents the shape of the vertical velocity profile. These equations are solved numerically using a finite volume scheme (Naaim, 1998). Classically, α_{sv} and k_{sv} were set to 1 for the entire study.

Traditionally (Salm et al., 1990), it is assumed that the coefficient μ summarizes snow properties as a function of e.g., altitude or exposure, whereas ξ is assimilated to a morphological parameter representing the roughness of the path. This interpretation of the Voellmy equation continues to be discussed (e.g., Ancy and Meunier, 2004), since it is not always fulfilled when calibration is undertaken on large data samples (Naaim et al., 2013). On the other hand, some theoretical justifications in its favor have been provided (Salm, 1993). We do not want to close the debate here, and adopt this simplification for a pragmatic reason: with regard to having two coefficients to estimate for each

event, only $n + 1$ unknowns have to be estimated from the data. Hence, μ_i , $i \in [1, n]$ are modeled as latent variables describing the random effects from one avalanche to another, and ξ as a parameter in the very statistical sense of the term.

Regarding probabilistic modeling of avalanche activity, avalanche frequency is assumed to be a Poisson distributed process (Eckert et al., 2007a), with its single parameter λ quantifying the mean annual avalanche number:

$$a|\lambda \sim P(\lambda) \quad (8)$$

The magnitude model embeds the propagation model within several probabilistic operators describing the variability of the different input–output quantities. First, the release abscissa x_{start} that corresponds to the beginning of the release zone is assumed to be purely random, and a Beta-distribution is a flexible choice to model various release zones behaviors (Meunier et al., 2001). However, since the Beta distribution is defined on the $]0, 1[$ interval, a little restrictive normalization is necessary. The length of the release zone is used, so that the normalized release position x_{startn} is:

$$x_{startn}|a_1, a_2 = \frac{x_{start} - x_{min}}{x_{max} - x_{min}} | a_1, a_2 \sim \text{Beta}(a_1, a_2) \quad (9)$$

where x_{max} and x_{min} are the maximal and minimal abscissas of the release zone that were estimated for the two case studies using simple topographical thresholds, and (a_1, a_2) the two parameters of the Beta distribution corresponding to each data set.

Given the normalized release abscissa x_{startn} , the mean release depth x_{startn} is assumed to be gamma-distributed, with a parameterization reflecting the dependency of the snow depth on the release abscissa and a constant dispersion around the mean:

$$h_{start}|b_1, b_2, \sigma_h, x_{start} \sim \text{Gamma} \left(\frac{1}{\sigma_h^2} (b_1 + b_2 x_{startn})^2, \frac{1}{\sigma_h^2} (b_1 + b_2 x_{startn}) \right) \quad (10)$$

This model is chosen to represent the skewness of a hydrological variable such as snow depth (where values much higher than the mean are plausible) as well as the possible variation of snow depth with altitude through the parameters (b_1, b_2, σ_h) of the Gamma mixture corresponding to each data set. For both case studies, release depths and other release dimensions corresponding to past observations were derived from deposit volumes of the EPA records as detailed in Eckert et al. (2010c), and/or from snow cover simulations (Durand et al., 2009).

Given the normalized release abscissa and the flow depth, the latent friction coefficient μ is assumed to be normally distributed, with four parameters (c, d, e, σ) characterizing, for each case study, its dependency on the release abscissa and mean release depth and with a constant dispersion around the mean:

$$\mu|c, d, e, \sigma, x_{start}, h_{start} \sim N(c + dx_{startn} + eh_{start}, \sigma) \quad (11)$$

Small Gaussian differences between the observed runout distances $x_{stop_{data}}$ and the latent computed runout distances x_{stop} are postulated:

$$x_{stop_{data}} | \sigma_{num}, x_{stop} \sim N(x_{stop}, \sigma_{num}) \quad (12)$$

These differences can result from numerical errors due to the imperfection of the propagation model, and/or from observation errors. The standard deviation of these numerical errors σ_{num} is to be specified for model identifiability.

In summary, the proposed frequency model has only one parameter $\theta_F = \lambda$. Conversely, the magnitude model is relatively complex, with ten parameters $\theta_M = (a_1, a_2, b_1, b_2, \sigma_h, c, d, e, \sigma, \xi)$ and, for each avalanche, the latent friction coefficient μ and the computed runout distance x_{stop}

measured on the horizontal axis starting at the top of the path. The different input variables and the latent friction coefficient μ are explicitly modeled as dependent variables, so as to take possible correlations into account that may affect extreme events. The joint probability of the magnitude observations given parameters and latent variables is obtained by combining the different conditional distributions:

$$p(x_{start}, h_{start}, x_{stop_{data}} | \theta_M, \mu, x_{stop}, \sigma_{num}) \quad (13)$$

$$= p(x_{start} | a_1, a_2) p(h_{start} | b_1, b_2, \sigma_h, x_{start}) p(x_{stop_{data}} | \sigma_{num}, x_{stop})$$

μ appears in the right-hand side term only indirectly, by constraining the deterministic propagation and the runout distance x_{stop} .

Appendix B. Bayesian calibration on historical data and posterior sampling

Under the magnitude–frequency independence hypothesis, the frequency and the magnitude models can be inferred separately. As detailed in (Eckert et al., 2010c), it is straightforward for the frequency model. For the magnitude model, the joint posterior of all unknown is:

$$p(\theta_M, \mu, x_{stop} | data, \sigma_{num}) \propto \pi(\theta_M) \times p(x_{start}, h_{start}, x_{stop_{data}} | \theta_M, \mu, x_{stop}, \sigma_{num}) \times p(\mu, x_{stop} | \theta_M, x_{start}, h_{start}, x_{stop_{data}}, \sigma_{num}) \quad (14)$$

where *data* denotes all observations $(x_{start_1}, h_{start_1}, x_{stop_{data_1}}, \dots, x_{start_N}, h_{start_N}, x_{stop_{data_N}})$. $\pi(\theta_M)$ is the prior distribution detailed in text and

Table 1. $p(x_{start}, h_{start}, x_{stop_{data}} | \theta_M, \mu, x_{stop}, \sigma_{num}) = \prod_{i=1}^n (p(x_{start_i}, h_{start_i}, x_{stop_{data_i}} | \theta_M, \mu, x_{stop}, \sigma_{num}))$ is the likelihood of the independent triplets $(x_{start_i}, h_{start_i}, x_{stop_{data_i}})$, $i \in [1, n]$. $p(\mu, x_{stop} | \theta_M, x_{start}, h_{start}, x_{stop_{data}}, \sigma_{num})$, the probability of the latent variables given parameters and observations, is given by the model specification (Eq. (11)) combined with the deterministic propagation.

Numerical implementation was carried out using Markov Chain Monte Carlo schemes. Specifically, the Metropolis–Hasting algorithm (Metropolis et al., 1953) fully detailed in Eckert et al. (2010c) was used, and convergence was carefully tested and granted using different chains starting at different point of the parameter space.

From the posterior mean $\hat{\theta}_M, \hat{\lambda}$, the Bayesian estimator of the parameters of our model under the classic hypothesis of a quadratic loss function, $p(y|\hat{\theta}_M)$ and $p(a|\hat{\theta}_F)$ were obtained for both case studies. These distributions quantify the randomness of the process studied given the data. For $p(y|\hat{\theta}_M)$ that includes the marginal distribution of some variables of interest for hazard zoning (runout distance, velocity, flow depth, see Fig. 3 for the Château Jouan case), a statistical-dynamical Monte Carlo approach is needed to obtain the distribution of the outputs of the numerical avalanche propagation model given the distribution of its inputs. The specified conditional distributions have to be used to integrate over the distribution of the latent friction coefficient μ :

$$p(y|\hat{\theta}_M) = \int p(x_{start} | \hat{a}_1, \hat{a}_2) \times p(h_{start} | \hat{b}_1, \hat{b}_2, \hat{\sigma}_h, x_{start}) \times p(x_{stop} | x_{start}, h_{start}, \mu, \hat{\xi}) \times d\mu \quad (15)$$

This was easily carried out in the numerical Monte Carlo set-up by propagating each set of simulated input variables.

References

Alestalo, J., 1971. Dendrochronological interpretation of geomorphic processes. *Fennia* 105, 1–139.

- Ancey, C., 2005. Monte Carlo calibration of avalanches described as Coulomb fluid flows. *Philos. Trans. R. Soc.* 363 (1832), 1529–1550.
- Ancey, C., 2012. Are there “dragon-kings” events (i.e. genuine outliers) among extreme avalanches? *Eur. Phys. J. Spec. Top.* 205, 117–129.
- Ancey, C., Meunier, M., 2004. Estimating bulk rheological properties of flowing snow avalanches from field data. *J. Geophys. Res.* 109.
- Ancey, C., Meunier, M., Richard, D., 2003. Inverse problem in avalanche dynamics models. *Water Resour. Res.* 39.
- Ancey, C., Gervasoni, C., Meunier, M., 2004. Computing extreme avalanches. *Cold Reg. Sci. Technol.* 39, 161–180.
- Barbolini, M., Keylock, C.J., 2002. A new method for avalanche hazard mapping using a combination of statistical and deterministic models. *Nat. Hazards Earth Syst. Sci.* 2, 239–245.
- Bartelt, P., Stöckli, V., 2001. The influence of tree and branch fracture, overturning and debris entrainment on snow avalanche flow. *Ann. Glaciol.* 32, 209–216.
- Bartelt, P., Bühler, Y., Buser, O., Christen, M., Meier, L., 2012. Modeling mass-dependent flow regime transitions to predict the stopping and depositional behavior of snow avalanches. *J. Geophys. Res.* 117.
- Bayes, M., Price, M., 1763. An essay towards solving a problem in the doctrine of chances. By the late rev. Mr. Bayes, F. R. S. Communicated by Mr. Price, in a letter to John Canton, A. M. F. R. S. *Philos. Trans. R. Soc. Lond.* 53, 370–418.
- Bebi, P., Kulakowski, D., Rixen, C., 2009. Snow avalanche disturbances in forest ecosystems – State of research and implications for management. *For. Ecol. Manag.* 257, 1883–1892.
- Bergue, M., 2000. P.P.R. Révision partielle du plan de prévention des risques naturels prévisibles - Commune de Chamonix Mont-Blanc.
- Bollschweiler, M., Stoffel, M., Schnewly, D.M., Bourqui, K., 2008. Traumatic resin ducts in *Larix decidua* stems impacted by debris flows. *Tree Physiol.* 28, 255–263.
- Bovis, M.J., Mears, A.J., 1976. Statistical prediction of snow avalanche runout from terrain variables in Colorado. *Arct. Alp. Res.* 8, 115–120.
- Bozhinskiy, A.N., Nazarov, A.N., Chernouss, P.A., 2001. Avalanches: a probabilistic approach to modelling. *Ann. Glaciol.* 32, 255–258.
- Butler, D.R., Malanson, G.P., 1985. A history of high-magnitude snow avalanches, southern Glacier National Park, Montana, USA. *Mt. Res. Dev.* 5, 175–182.
- Butler, D.R., Sawyer, C.F., 2008. Dendrogeomorphology and high-magnitude snow avalanches: A review and case study. *Nat. Hazards Earth Syst. Sci.* 8, 303–309.
- Butler, D.R., Sawyer, C.F., Maas, J.A., 2010. Tree-ring dating of snow avalanches in Glacier National Park, Montana, USA. In: Stoffel, M., Bollschweiler, M., Butler, D.R., Luckman, B.H. (Eds.), *Tree Rings and Natural Hazards*. Springer Netherlands, Dordrecht, pp. 35–46.
- Castebrunet, H., Eckert, N., Giraud, G., 2012. Snow and weather climatic control on snow avalanche occurrence fluctuations over 50 yr in the French Alps. *Clim. Past* 8, 855–875.
- Casteller, A., Christen, M., Villalba, R., Martínez, H., Stöckli, V., Leiva, J.C., Bartelt, P., 2008. Validating numerical simulations of snow avalanches using dendrochronology: The Cerro Ventana event in Northern Patagonia, Argentina. *Nat. Hazards Earth Syst. Sci.* 8, 433–443.
- Corona, C., Rovéra, G., Lopez Saez, J., Stoffel, M., Perfettini, P., 2010. Spatio-temporal reconstruction of snow avalanche activity using tree rings: Pierres Jean Jeanne avalanche talus, Massif de l’Oisans, France. *Catena* 83, 107–118.
- Corona, C., Lopez Saez, J., Stoffel, M., Bonnefoy, M., Richard, D., Astrade, L., Berger, F., 2012a. How much of the real avalanche activity can be captured with tree rings? An evaluation of classic dendrogeomorphic approaches and comparison with historical archives. *Cold Reg. Sci. Technol.* 74–75, 31–42.
- Corona, C., Lopez Saez, J., Stoffel, M., Rovera, G., Edouard, J.-L., Berger, F., 2012b. Seven centuries of avalanche activity at Echalp (Queyras massif, southern French Alps) as inferred from tree rings. *The Holocene* 23, 292–304.
- Corona, C., Trappmann, D., Stoffel, M., 2013. Parameterization of rockfall source areas and magnitudes with ecological recorders: When disturbances in trees serve the calibration and validation of simulation runs. *Geomorphology* 202, 33–42.
- Delparte, D., Jamieson, B., Waters, N., 2008. Statistical runout modeling of snow avalanches using GIS in Glacier National Park, Canada. *Cold Reg. Sci. Technol.* 54, 183–192.
- Durand, Y., Laternser, M., Giraud, G., Etchevers, P., Lesaffre, B., Mérindol, L., 2009. Reanalysis of 44 yr of climate in the French Alps (1958–2002): methodology, model validation, climatology, and trends for air temperature and precipitation. *J. Appl. Meteorol. Climatol.* 48, 429–449.
- Eckert, N., Parent, E., Bélanger, L., Garcia, S., 2007a. Hierarchical Bayesian modelling for spatial analysis of the number of avalanche occurrences at the scale of the township. *Cold Reg. Sci. Technol.* 50, 97–112.
- Eckert, N., Parent, E., Richard, D., 2007b. Revisiting statistical–topographical methods for avalanche predetermination: Bayesian modelling for runout distance predictive distribution. *Cold Reg. Sci. Technol.* 49, 88–107.
- Eckert, N., Parent, E., Faug, T., Naaim, M., 2008a. Optimal design under uncertainty of a passive defense structure against snow avalanches: from a general Bayesian framework to a simple analytical model. *Nat. Hazards Earth Syst. Sci.* 8, 1067–1081.
- Eckert, N., Parent, E., Naaim, M., Richard, D., 2008b. Bayesian stochastic modelling for avalanche predetermination: From a general system framework to return period computations. *Stoch. Env. Res. Risk A.* 22, 185–206.
- Eckert, N., Parent, E., Faug, T., Naaim, M., 2009. Bayesian optimal design of an avalanche dam using a multivariate numerical avalanche model. *Stoch. Env. Res. Risk A.* 23, 1123–1141.
- Eckert, N., Baya, H., Deschatres, M., 2010a. Assessing the response of snow avalanche runout altitudes to climate fluctuations using hierarchical modeling: Application to 61 winters of data in France. *J. Clim.* 23, 3157–3180.
- Eckert, N., Coleou, C., Castebrunet, H., Deschatres, M., Giraud, G., Gaume, J., 2010b. Cross-comparison of meteorological and avalanche data for characterising avalanche cycles:

- The example of December 2008 in the eastern part of the French Alps. *Cold Reg. Sci. Technol.* 64, 119–136.
- Eckert, N., Naaim, M., Parent, E., 2010c. Long-term avalanche hazard assessment with a Bayesian depth-averaged propagation model. *J. Glaciol.* 56, 563–586.
- Eckert, N., Keylock, C.J., Castebrunet, H., Lavigne, A., Naaim, M., 2013. Temporal trends in avalanche activity in the French Alps and subregions: from occurrences and runout altitudes to unsteady return periods. *J. Glaciol.* 59, 93–114.
- ESRI, 2013. ArcGIS. <http://www.esri.com/software/arcgis/>.
- Feistl, T., Bebi, P., Bühler, Y., Christen, M., Teich, M., Bartelt, P., 2012. Stopping behavior of snow avalanches in forests. *Proceedings of the International Snow Science Workshop ISSW*. Anchorage, Alaska, pp. 420–426.
- Fischer, J.-T., Fromm, R., Gauer, P., Sovilla, B., 2013. Evaluation of probabilistic snow avalanche simulation ensembles with Doppler radar observations. *Cold Reg. Sci. Technol.* 97, 151–158.
- Gauer, P., Medina-Cetina, Z., Lied, K., Kristensen, K., 2009. Optimization and probabilistic calibration of avalanche block models. *Cold Reg. Sci. Technol.* 59, 251–258.
- Germain, D., Filion, L., Héту, B., 2005. Snow avalanche activity after fire and logging disturbances, northern Gaspé Peninsula, Quebec, Canada. *Can. J. Earth Sci.* 42, 2103–2116.
- Germain, D., Héту, B., Filion, L., 2010. Tree-ring based reconstruction of past snow avalanche events and risk assessment in Northern Gaspé Peninsula (Québec, Canada). In: Stoffel, M., Bollschweiler, M., Butler, D.R., Luckman, B.H. (Eds.), *Tree Rings and Natural Hazards*. Springer Netherlands, Dordrecht, pp. 51–73.
- Grêt-Regamey, A., Straub, D., 2006. Spatially explicit avalanche risk assessment linking Bayesian networks to a GIS. *Nat. Hazards Earth Syst. Sci.* 6, 911–926.
- Hazen, A., 1914. Storage to be provided in impounding reservoirs for municipal water supply. *Trans. Am. Assoc. Civ. Eng.* 77.
- Issler, D., 1998. Modelling of snow entrainment and deposition in powder-snow avalanches. *Ann. Glaciol.* 26, 253–258.
- Jamard, A.-L., Garcia, S., Bélanger, L., 2002. L'Enquête Permanente sur les Avalanches (EPA) - Statistique descriptive générale des événements et des sites.
- Jomelli, V., Pech, P., 2004. Effects of the Little Ice Age on avalanche boulder tongues in the French Alps (Massif des Ecrins). *Earth Surf. Process. Landf.* 29, 553–564.
- Jomelli, V., Delval, C., Grancher, D., Escande, S., Brunstein, D., Hetu, B., Filion, L., Pech, P., 2007. Probabilistic analysis of recent snow avalanche activity and weather in the French Alps. *Cold Reg. Sci. Technol.* 47, 180–192.
- Keylock, C.J., 2005. An alternative form for the statistical distribution of extreme avalanche runout distances. *Cold Reg. Sci. Technol.* 42, 185–193.
- Keylock, C.J., McClung, D.M., Mar Magnússon, M., 1999. Avalanche risk mapping by simulation. *J. Glaciol.* 45, 303–314.
- Kogelnig-Mayer, B., Stoffel, M., Schneuwly-Bollschweiler, M., 2013. Four-dimensional growth response of mature *Larix decidua* to stem burial under natural conditions. *Trees* 27, 1217–1223.
- Latenser, M., Schneebeli, M., 2002. Temporal trend and spatial distribution of avalanche activity during the last 50 years in Switzerland. *Nat. Hazards* 27, 201–230.
- Lied, K., Bakkehoi, S., 1980. Empirical calculations of snow-avalanche run-out distance based on topographic parameters. *J. Glaciol.* 26, 165–177.
- Luckman, B.H., 2010. Dendrogeomorphology and snow avalanche research. In: Stoffel, M., Bollschweiler, M., Butler, D.R., Luckman, B.H. (Eds.), *Tree Rings and Natural Hazards*. Springer Netherlands, Dordrecht, pp. 27–34.
- Malanson, G.P., Butler, D.R., 1984. Transverse pattern of vegetation on avalanche paths in the northern Rocky Mountains, Montana. *Great Basin Nat.* 44, 453–458.
- Martin, E., Giraud, G., Lejeune, Y., Boudart, G., 2001. Impact of a climate change on avalanche hazard. *Ann. Glaciol.* 32, 163–167.
- McClung, D.M., 1990. A model for scaling avalanche speeds. *J. Glaciol.* 36, 188–198.
- McClung, D.M., 2000. Extreme avalanche runout in space and time. *Can. Geotech. J.* 37, 161–170.
- McClung, D.M., 2003. Magnitude and frequency of avalanches in relation to terrain and forest cover. *Arct. Antarct. Alp. Res.* 35, 82–90.
- McClung, D.M., Lied, K., 1987. Statistical and geometrical definition of snow avalanche runout. *Cold Reg. Sci. Technol.* 13, 107–119.
- McClung, D.M., Schaerer, P.A., 1985. Characteristics of flowing snow and avalanche impact pressures. *Ann. Glaciol.* 6, 9–14.
- McClung, D.M., Schaerer, P.A., 2006. *The avalanche handbook*, The Mountaineers Books 3rd Revise ed.
- Mears, A.I., 1989. Avalanche runout distances and dynamics: current methods and limitations. *Avalanche Rev.* 7.
- Mears, A.I., 1992. Snow-avalanche hazard analysis for land-use planning and engineering. *Colo. Geol. Surv.* 59.
- Metropolis, N., Rosenbluth, A.W., Rosenbluth, M.N., Teller, A.H., Teller, E., 1953. Equation of state calculations by fast computing machines. *J. Chem. Phys.* 21, 1087–1092.
- Meunier, M., Ancey, C., 2004. Towards a conceptual approach to predetermining long-return-period avalanche run-out distances. *J. Glaciol.* 50, 268–278.
- Meunier, M., Ancey, C., Naaim, M., 2001. Mise au point d'une méthode de prédétermination statistique des côtes d'arrêt d'avalanches. *La Houille Blanche* 92–98.
- Mougin, P., 1922. *Etudes glaciologiques: Les avalanches en Savoie*, Etudes glaciologiques. Imprimerie Nationale, Paris.
- Naaim, M., 1998. Contribution to snow drift and avalanches flows modelling. (Habilitation thesis) Université Joseph Fourier.
- Naaim, M., Naaim-Bouvet, F., Faug, T., Bouchet, A., 2004. Dense snow avalanche modeling: Flow, erosion, deposition and obstacle effects. *Cold Reg. Sci. Technol.* 39, 193–204.
- Naaim, M., Faug, T., Naaim-Bouvet, F., Eckert, N., 2010. Return period calculation and passive structure design at the Taconnaz avalanche path (France). *Ann. Glaciol.* 51, 89–97.
- Naaim, M., Durand, Y., Eckert, N., Chambon, G., 2013. Dense avalanche friction coefficients: influence of physical properties of snow. *J. Glaciol.* 59, 771–782.
- Pederson, G.T., Reardon, B.A., Caruso, C.J., Fagre, D.B., 2006. High resolution tree-ring based spatial reconstructions of snow avalanche activity in glacier national park, Montana, USA. *Proceedings of the International Snow Science Workshop ISSW*. Telluride, CO, pp. 436–443.
- Reardon, B.A., Pederson, G.T., Caruso, C.J., Fagre, D.B., 2008. Spatial reconstructions and comparisons of historic snow avalanche frequency and extent using tree rings in Glacier National Park, Montana, U.S.A. *Arct. Antarct. Alp. Res.* 40, 148–160.
- Rognon, P.G., Chevoir, F., Bellot, H., Ousset, F., Naaim, M., Cousot, P., 2008. Rheology of dense snow flows: Inferences from steady state chute-flow experiments. *J. Rheol.* 52, 729.
- Salm, B., 1993. Flow, flow transition and runout distances of flowing avalanches. *Ann. Glaciol.* 18, 221–226.
- Salm, B.W., Burkhard, A., Gubler, H.U., 1990. Berechnungen von Fließlawinen: Eine Anleitung für Praktiker mit Beispielen.
- Savage, S.B., Hutter, K., 1989. The motion of a finite mass of granular material down a rough incline. *J. Fluid Mech.* 199, 177–215.
- Schläpky, R., Jomelli, V., Grancher, D., Stoffel, M., Corona, C., Brunstein, D., Eckert, N., Deschatres, M., 2013. A new tree-ring-based, semi-quantitative approach for the determination of snow avalanche events: use of classification trees for validation. *Arct. Antarct. Alp. Res.* 45, 383–395.
- Schneuwly, D.M., Stoffel, M., Bollschweiler, M., 2009a. Formation and spread of callus tissue and tangential rows of resin ducts in *Larix decidua* and *Picea abies* following rockfall impacts. *Tree Physiol.* 29, 281–289.
- Schneuwly, D.M., Stoffel, M., Dorren, L., Berger, F., 2009b. Three-dimensional analysis of the anatomical growth response of European conifers to mechanical disturbance. *Tree Physiol.* 29, 1247–1257.
- Stoffel, M., Bollschweiler, M., 2008. Tree-ring analysis in natural hazards research – an overview. *Nat. Hazards Earth Syst. Sci.* 8, 187–202.
- Stoffel, M., Bollschweiler, M., 2009. Tree-ring reconstruction of past debris flows based on a small number of samples—possibilities and limitations. *Landslides* 6, 225–230.
- Stoffel, M., Hitz, O.M., 2008. Rockfall and snow avalanche impacts leave different anatomical signatures in tree rings of juvenile *Larix decidua*. *Tree Physiol.* 28, 1713–1720.
- Stoffel, M., Perret, S., 2006. Reconstructing past rockfall activity with tree rings: Some methodological considerations. *Dendrochronologia* 24, 1–15.
- Stoffel, M., Bollschweiler, M., Hassler, G., 2006. Differentiating past events on a cone influenced by debris-flow and snow avalanche activity – a dendrogeomorphological approach. *Earth Surf. Process. Landf.* 31, 1424–1437.
- Stoffel, M., Bollschweiler, M., Butler, D.R., Luckman, B.H., 2010. *Tree Rings and Natural Hazards*. Springer Netherlands, Dordrecht.
- Stoffel, M., Butler, D.R., Corona, C., 2013. Mass movements and tree rings: A guide to dendrogeomorphic field sampling and dating. *Geomorphology* 200, 106–120.
- Straub, D., Grêt-Regamey, A., 2006. A Bayesian probabilistic framework for avalanche modelling based on observations. *Cold Reg. Sci. Technol.* 46, 192–203.
- Takeuchi, Y., Torita, H., Nishimura, K., Hirashima, H., 2011. Study of a large-scale dry slab avalanche and the extent of damage to a cedar forest in the Makunosawa valley, Myoko, Japan. *Ann. Glaciol.* 52, 119–128.
- Teich, M., Bartelt, P., Grêt-Regamey, A., Bebi, P., 2012. Snow avalanches in forested terrain: Influence of forest parameters, topography, and avalanche characteristics on runout distance. *Arct. Antarct. Alp. Res.* 44, 509–519.
- Timell, T., 1986. *Compression wood in Gymnosperms*. Springer, Berlin.
- Trappmann, D., Stoffel, M., 2013. Counting scars on tree stems to assess rockfall hazards: A low effort approach, but how reliable? *Geomorphology* 180–181, 180–186.
- Van der Burght, L., Stoffel, M., Bigler, C., 2012. Analysis and modelling of tree succession on a recent rockslide deposit. *Plant Ecol.* 213, 35–46.
- Voellmy, A., 1955. Über die Zerstörungskraft den Lawinen. *Schweiz. Bauzeitung* 73, 159–162 (212–217, 246–249 and 280–285).
- Vriend, N.M., McElwaine, J.N., Sovilla, B., Keylock, C.J., Ash, M., Brennan, P.V., 2013. High-resolution radar measurements of snow avalanches. *Geophys. Res. Lett.* 40, 727–731.
- Weir, P., 2002. Snow avalanche management in forested terrain. *Res. Br., B.C. Min. For.* Victoria, B.C.